DOT/FAA/AR-01/27, II

Office of Aviation Research
Washington, D.C. 20591

Engine Debris Fuselage Penetration Testing Phase II

September 2002

Final Report

This document is available to the U.S. public through the National Technical Information Service (NTIS), Springfield, Virginia 22161.

U.S. Department of Transportation
Federal Aviation Administration

NOTICE

Technical Report Documentation Page

1. Report No.	2. Government Accession No.	3. Recipient's Catalog No.
DOT/FAA/AR-01/27, II		

4. Title and Subtitle	5. Report Date
ENGINE DEBRIS FUSELAGE PENETRATION TESTING, PHASE II	September 2002
	6. Performing Organization Code NAWCWD 418300D
7. Author(s) Steven J. Lundin	8. Performing Organization Report No.
9. Performing Organization Name and Address Commander Naval Air Warfare Center Weapons Division 1 Administration Way China Lake, CA 93555-6001	10. Work Unit No. (TRAIS) 11. Contract or Grant No.
12. Sponsoring Agency Name and Address U.S. Department of Transportation Federal Aviation Administration Office of Aviation Research Washington, DC 20591	13. Type of Report and Period Covered Final Report 14. Sponsoring Agency Code ANM-100

15. Supplementary Notes

The FAA, William J. Hughes Technical Center COTR's: William Emmerling and Donald Altobelli

16. Abstract

During October and November 2000 the Naval Air Warfare Center, China Lake conducted a series of simulated uncontained engine failure structural impact tests. A large 12-inch gas gun was used to launch turbojet engine fan blade segments into a narrow-body commercial aircraft fuselage. The impacts were documented and analyzed with high-speed photography. Impact velocities, presented areas, and residual velocities were calculated. These data were then compared to analytic results predicted by the Joint Technical Coordinating Group for Munitions Effectiveness (JTCG/ME) penetration equations. The results are presented in this report.

17. Key Words	18. Distribution Statement
Engine debris, Mitigation testing, Uncontained, Fuselage penetration	This document is available to the public through the National Technical Information Service (NTIS), Springfield, Virginia 22161.

19. Security Classif. (of this report)	20. Security Classif. (of this page)	21. No. of Pages	22. Price
Unclassified	Unclassified	82	

Form DOT F1700.7 (8-72) Reproduction of completed page authorized

TABLE OF CONTENTS

EXECUTIVE SUMMARY vii

1. INTRODUCTION 1

1.1 Purpose 1
1.2 Background 1

1.2.1 Penetration Methodologies 1
1.2.2 The JTCG/ME Penetration Equations 2
1.2.3 The FAA V_{50} Equation 3

1.3 Related Activities/Documents 3

2. DISCUSSION OF TEST AND TEST RESULTS 4

2.1 Test Setup 5
2.2 Test Procedure 10
2.3 Presented Area Measurement Methodology 11
2.4 Test Results 13

2.4.1 Analysis Discussion 13
2.4.2 Results 14

2.5 Summary 19
2.6 Future Plans 20

3. REFERENCES 20

APPENDICES

A—Dimensional Analysis of Penetration Equations

B—A Study of Improvements to the Existing Penetration Equations to Include the Effects of Structural Elements

LIST OF FIGURES

Figure		Page
1	Barrier Installation	4
2	Typical Interior View of Target Areas	5
3	Phase II Test Setup	5
4	Medium Fragment, 1.0 lb Fan Blade Segment	7
5	Large Fragment, 1.76 lb Fan Blade Segment	7
6	Small Fragment, 0.67 lb Fan Blade Fragment	8
7	Disk Fragment Impact, Exterior View	8
8	Large Fragment Impact, Interior View	9
9	Barrier Test Showing Captured Fragment	9
10	Barrier Impact Showing a Penetrated Interior Wall Panel	10
11	Left Hand Reference Frame	12
12	Fragment Yaw Definition	12
13	Fragment Pitch Definition	13
14	Fragment Roll Definition	13
15	Typical Structural Elements	15
16	Test 1 Results, JTCG Equations for V_{50} and V_r Used	16
17	Test 1 Results, FAA Equation for V_{50} and JTCG V_r Equation Used	16
18	JTCG Equations With Other Structure Modeled as Second Plate	17
19	FAA V_{50} Equation With JTCG V_r Plugging Equation and No Secondary Structure Modeling (Single Plate Model)	17
20	JTCG Equations With Secondary Structure Modeled as Second Plate	18
21	JTCG Equations Without Secondary Structure	18
22	FAA V_{50} Equation With JTCG V_r Plugging Equation and No Secondary Structure Modeling (Multiple Plate Model)	19

LIST OF TABLES

Table		Page
1	Dynamic Shear Moduli For Steel and Aluminum	3
2	Fragment Orientations and Obliquities	6
3	Penetration Equations Input Parameters	14

EXECUTIVE SUMMARY

This work was conducted under the sponsorship and oversight of the Federal Aviation Administration (FAA) Engine and Propeller Directorate and the Transport Airplane Directorate. The Uncontained Engine Debris Mitigation Program falls under the Catastrophic Failure Prevention Program which is lead by the FAA William J. Hughes Technical Center.

During October and November 2000 the Naval Air Warfare Center Weapons Division, China Lake, conducted a series of structural impact tests to simulate uncontained engine failures. A large 12-inch gas gun was used to launch turbine engine fan blade segments into a narrow-body commercial aircraft fuselage. The impacts were documented and analyzed with high-speed photography. Impact velocities, presented areas, and residual velocities were calculated. The data were then compared to analytic results predicted by the Joint Technical Coordinating Group for Munitions Effectiveness penetration equations and the FAA equation for ballistic limit (V_{50}). The comparison indicates that very good estimations of residual energies are possible for most impact areas on a commercial structure.

1. INTRODUCTION.

1.1 PURPOSE.

The goal of this work was to determine a simple methodology for estimating residual energies of engine debris for impacts of simple and complex aircraft structures.

1.2 BACKGROUND.

The damaging effects from an uncontained aircraft turbine engine failure can be catastrophic. As a result, the Federal Aviation Administration (FAA) has commissioned a program, The Uncontained Engine Debris Mitigation Program, to mitigate the damaging effects of such an event. This will work with industry and government to determine possible engineering solutions to this problem.

As part of this program, the Naval Air Warfare Center Weapons Division (NAWCWD) has been tasked to evaluate ballistic damage analysis tools and techniques which are currently in use by the defense community. The intent is to determine their applicability in predicting the damaging effects from an uncontained engine failure. This report documents testing which was conducted in the evaluation of these tools and techniques.

The FAA fuselage tests started in March 1999 as Phase I. This work is a continuation of the work documented in reference 1 and extends the database of large fragment impacts into mid-size commercial aircraft structures. Phase I impacted small (0.3 lb) to medium (0.7 lb) size fragments into a commercial aircraft fuselage at varied locations. Most of these impacts were against the fuselage skin only. The results of these tests showed that the penetration model had excellent agreement with the experimental data in the skin category of shots. Fragment impacts of the ribs and stringers did not correlate as well. From that work, it was recommended that a second series of shots be conducted to expand the rib and stringer categories while including larger fragments.

Phase II testing impacted complex structure with medium (0.7 lb) to large (1.8 lb) fragments. Three large (3.0 lb) disk fragments.

1.2.1 Penetration Methodologies.

For over 35 years, a lot of research has been done on ballistic impacts of aircraft structures. Most of this research has been done for ordnance warhead fragments, which are small in comparison to engine debris sizes studied here. Three previous research efforts have been conducted: the John's Hopkins University Project THOR [2], Joint Technical Coordination Group for Munitions Effectiveness (JTCG/ME) Penetration Equations [3], and an equation known as the FAA Energy Equation [4]. The THOR and JTCG equations were examined extensively. The JTCG equations were found to be nondimensional forms of the THOR equations. The THOR equations have been used since 1961 as the defacto baseline for penetration of metals by projectiles. The THOR work used very small (0.0007-0.12 lb) cylinders to impact into a variety of metal plates. Impact conditions were mostly at very high speeds (1000-12000 ft/s with the bulk of the data in the 4000-5000 ft/s range). This research was generally considered excellent and a good empirical model was developed for the data that was collected. In considering the impacts of large relatively flat plates into a metal structure at velocities of 300-800 ft/s, one should not expect the THOR equations to provide a suitable estimate of the impact's residual energies. The THOR and JTCG were the only equations available and provided a starting point for this research.

One parameter that goes into the penetration equations is V_{50}. This is the velocity for which 50% of the impacts will penetrate the material, which is determined by extensive testing of material samples or may be estimated from a formula. The THOR and JTCG equations require a V_{50} for the computation of residual velocity. The FAA V_{50} equation was found not to be the same as the THOR V_{50} equation. The difference between the two is that the THOR form uses the presented area and the FAA form uses the perimeter of the presented area. This will be shown to be very valuable to this work.

1.2.2 The JTCG/ME Penetration Equations.

Among the analysis tools currently in use are the JTCG/ME penetration equations. The JTCG/ME work used the THOR equations in a nondimensional form. The JTCG/ME penetration equations are as follows.

The residual velocity equation:

$$V_r = \frac{\sqrt{V^2 - V_{50}^2}}{1.0 + \dfrac{\rho A_p t}{W \cos\theta}} \tag{1}$$

The ballistic limit equation:

$$V_{50} = C_{bf}\left(\frac{\rho_f t A_p}{W}\right)^{b_f} \sec^h\theta \left(\frac{\rho_f t A_p}{W_o}\right)^f \tag{2}$$

where:

V	=	debris initial velocity
V_{50}	=	debris ballistic limit velocity. Penetration occurs 50% of the time.
V_r	=	debris residual velocity
ρ_f	=	debris specific weight (debris weight/volume)
ρ	=	plate specific weight (plate weight/volume)
t	=	plate thickness
A_p	=	debris presented area along direction of travel
θ	=	obliquity (90° is edge on)
W	=	debris weight
W_o	=	100 grains
bf, h, f	=	empirical constants
C_{bf}	=	fragment specific variable

1.2.3 The FAA V_{50} Equation.

The relationship (shown in equation 3) was derived by equating the impact energy to the work done by shearing out a plug of a given circumference. The term G_d is called dynamic shear modulus in reference 4 but is more accurately named dynamic shear strength.

$$V_{50} = \sqrt{\frac{2 \cdot L \cdot G_d \cdot t^2}{m \cdot \cos^2 \theta}} \qquad (3)$$

where:

L = Presented area perimeter (m)
G_d = Dynamic shear modulus (Pa)
t = Target thickness (m)
m = Mass of fragment (kg)
θ = Obliquity of impact (deg; 90° is edge on)

The term G_d above is not a common materiel property. A literature search has been unable to obtain more values for the parameter than presented in reference 4 and shown below in table 1 . Appendix A contains a dimensional analysis of the penetration equations.

TABLE 1. DYNAMIC SHEAR MODULI FOR STEEL AND ALUMINUM

Material	Dynamic Shear Modulus G_d (psi)
Steel	188500
Aluminum	30450

The American Society for Testing and Materials describes a standard measurement method for dynamic shear modulus in reference 5.

The values in table 1 may have been determined empirically.

1.3 RELATED ACTIVITIES/DOCUMENTS.

In 1998, NAWCWD China Lake conducted its first series of impact tests for the FAA. That work is documented in reference 6. The first tests used flat aluminum plates and aircraft cowl sections as targets. The projectiles were small (3″ by 5″ and less) fan, compressor, and turbine blade fragments and a standard titanium simulated fragment. During February 1999, China Lake began a second set of tests using a mid-size commercial aircraft fuselage. Impacts to the fuselage were conducted with small- to medium-size fan blade fragments (up to 3″ by 8″). That work is documented in reference 1.

During Phase I and Phase II of the China Lake fuselage tests, scientists from SRI International conducted some experiments with Kevlar and Zylon re-enforcments on the interior wall panels of the aircraft. The objective of these experiments was to determine the number of sheets required to protect the passenger cabin from a 5″ by 7″ fan blade fragment traveling at 813 ft/s. The test results were somewhat successful and showed that 3-4 sheets of fabric could stop the fragment; however, the attachment to the fuselage needed further investigation. Complete SRI Phase I results are documented in reference 7 and the Phase II documentation is contained in reference 8. Figure 1 shows a typical barrier installation for the SRI test.

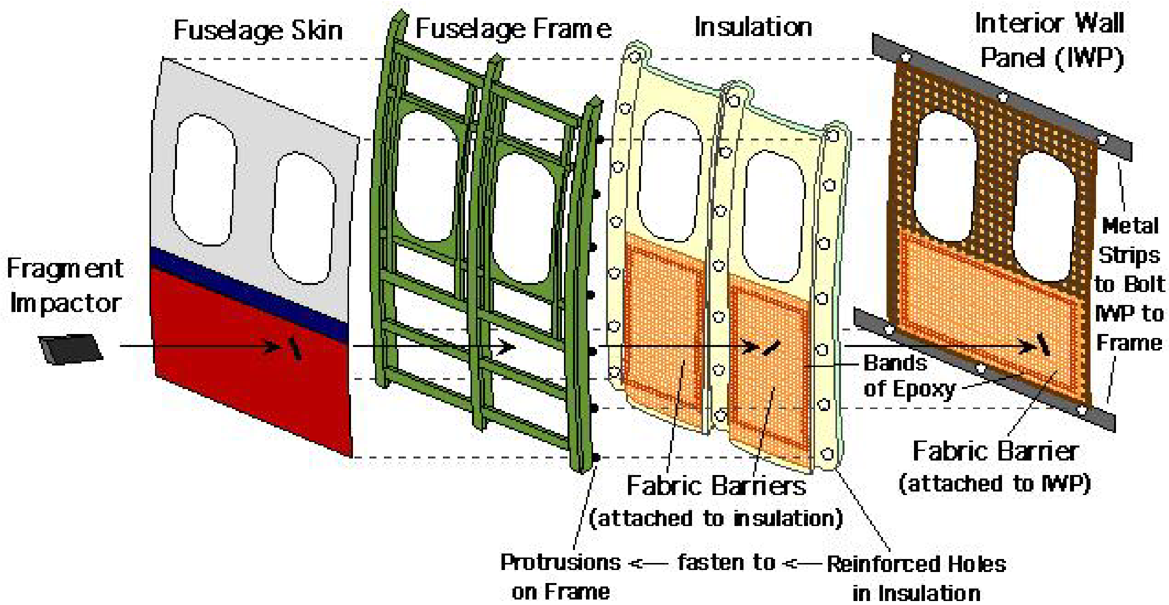

FIGURE 1. BARRIER INSTALLATION

2. DISCUSSION OF TEST AND TEST RESULTS.

The goal of this effort was to produce a numerically efficient algorithm for computing the residual velocities of large, flat projectiles characteristic of turbine engine debris. At the conclusion of the Phase I tests, there seemed to be a good solution to this problem. However, data was lacking on large fragments, therefore Phase II was initiated to collect impact data for 8″ by 8″ by 0.25″ fragments (approximately 1.8 pounds). The Phase II data did not correlate satisfactorily with the JTCG/ME penetration equations even after several attempts at modifying the equations to accommodate partial impacts of secondary structures. (JTCG/ME penetration equation correlation with test data is provided in section 2.4.2.1.) The 8″ by 8″ projectiles usually impact stringers and/or ribs because the stringers have less than 8″ of vertical separation. Figure 2 shows the structure of the cabin area inside the aircraft used.

FIGURE 2. TYPICAL INTERIOR VIEW OF TARGET AREAS

2.1 TEST SETUP.

A midsize commercial aircraft fuselage center section approximately 40 ft. long was used as the target for these test shots. Figure 3 shows the test site setup with insets for the exterior and interior. The locations of the gas gun, cameras, and lights are typical. The fuselage could be rotated to approximately 30 degrees and translated such that the full length could be presented to the gun. Theatrical 1000 W lights were used to provide light for the high-speed 16 mm cameras. The cameras were run at 6000 frames per second and had a shutter speed of 1/15000th second. Based on the available lighting, this was the fastest speed possible to obtain usable high-speed film images.

FIGURE 3. PHASE II TEST SETUP

The projectiles were cut from turbine engine fan blades. These fragments were fired from a nitrogen gas gun at speeds ranging from 416 to 986 ft/s. The projectiles were launched with a sabot that gave a small amount of angular momentum to the fragments. This provided a highly accurate aim and good control of orientation at impact. Table 2 summarizes the test shots completed. The test objectives were to collect data for the large fan blade fragment impacts against the fuselage skin and various fuselage skin/stringer combinations.

TABLE 2. FRAGMENT ORIENTATIONS AND OBLIQUITIES

Shot No.	Shot Category	Blade Type	Pitch (deg)	Roll (deg)	Obliquity (deg)
1	Skin	7x4	1.8	32.5	0
2	Skin	7x4	-3.9	-9.4	0
3.1	Hat stringer	8x8	3.2	26.7	0
4	Hat, Z, skn-jnt	8x8	12.9	10.7	0
5	Hat stringer	8x8	-4.9	-1.3	0
8	disk frag hat	7x2	0.0	0.0	0
9	disk frag hat	7x2	0.0	0.0	0
10	disk frag	7x2	0.0	0.0	0
11.1	Z stringer	8x8	15.3	7.8	0
12	Z stringer	8x8	-5.0	15.0	0
14	Hat stringer	8x8	8.4	2.4	0
15	Hat stringer	8x8	41.0	0.0	0
16	hat stringer	8x8	-7.5	-30.4	0
18	SRI	4x3	-6.2	-19.0	0
19	SRI	4x3	-33.7	-26.0	0
20	SRI	4x3	-16.4	-12.4	0
21	SRI	4x3	21.9	12.8	0
22	SRI	7x6	10.0	27.0	0
23	Skin	7x6	3.0	25.0	0
24	Hat stringer	8x8	15.0	-18.3	14.9
25	Rib	8x8	28.9	28.2	14.9
26	Hat stringer	8x8	-18.2	-27.5	14.6
27	Skin	7x5	35.9	-62.9	14.9
28	Skin	7x5	50.5	-41.6	14.9
30	SRI	8x5	-48.8	-68.5	14.9
31	SRI	4x3	-26.9	-20.0	14.9
32	SRI	8x5	8.9	-3.4	14.9
33	SRI	8x5	-5.0	50.0	14.9
34	SRI	7x5	7.9	22.1	14.9
36	SRI	7x4	-6.6	3.5	14.9
37	Hat stringer	8x8	6.4	-58.9	14.9
38	Hat stringer	8x8	-20.0	-87.0	14.9
39	Hat stringer	8x8	25.5	-30.6	14.9
40	Hat stringer	8x8	16.3	-78.5	14.9
41	Hat stringer	8x8	7.4	60.0	14.9
42	Hat stringer	8x8	2.9	72.3	14.9

The photographs in figures 4 through 8 are indicative of the images made in documenting these tests. A companion CD-ROM containing the entire photographic database (approximately 600 images) is available from the Naval Air Warfare Center, China Lake.

Some of the barrier research conducted by SRI International is included in figures 9 and 10. See reference 8 for more details.

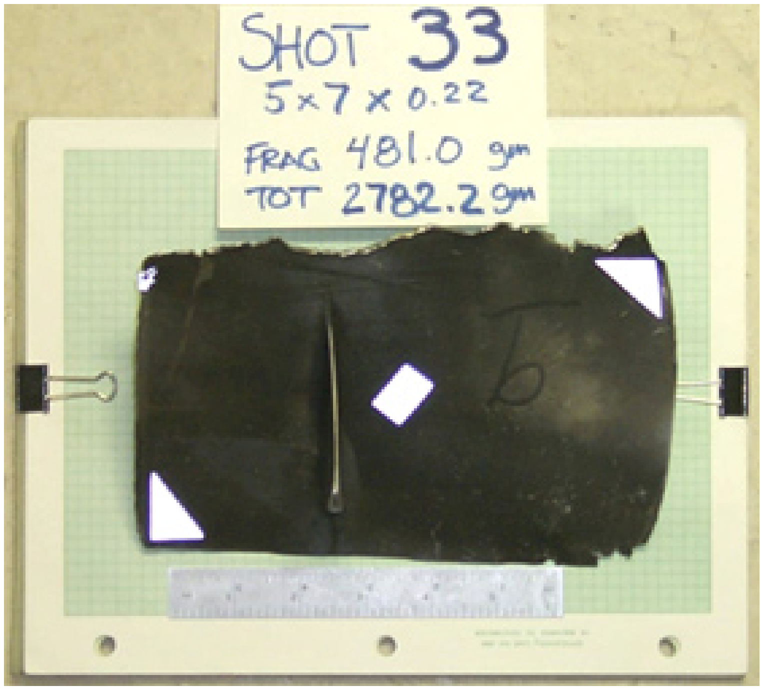

FIGURE 4. MEDIUM FRAGMENT, 1.0 lb FAN BLADE SEGMENT

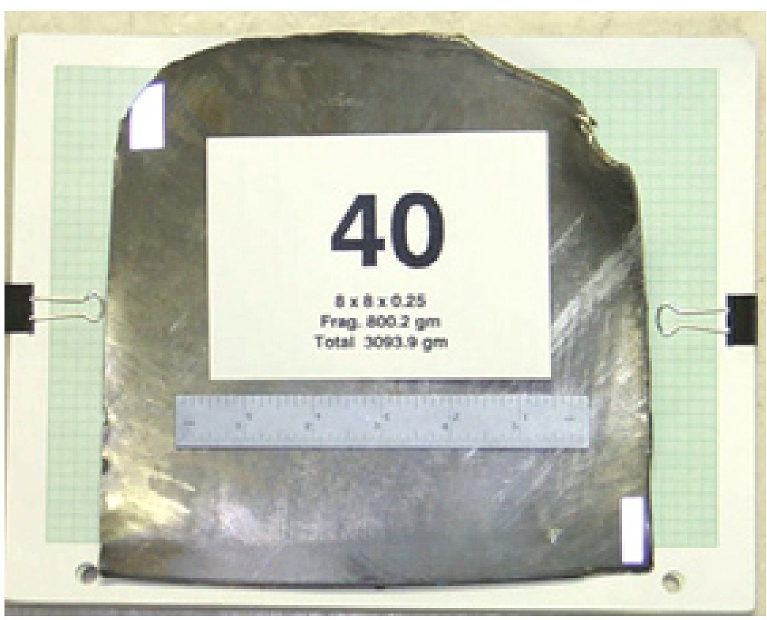

FIGURE 5. LARGE FRAGMENT, 1.76 lb FAN BLADE SEGMENT

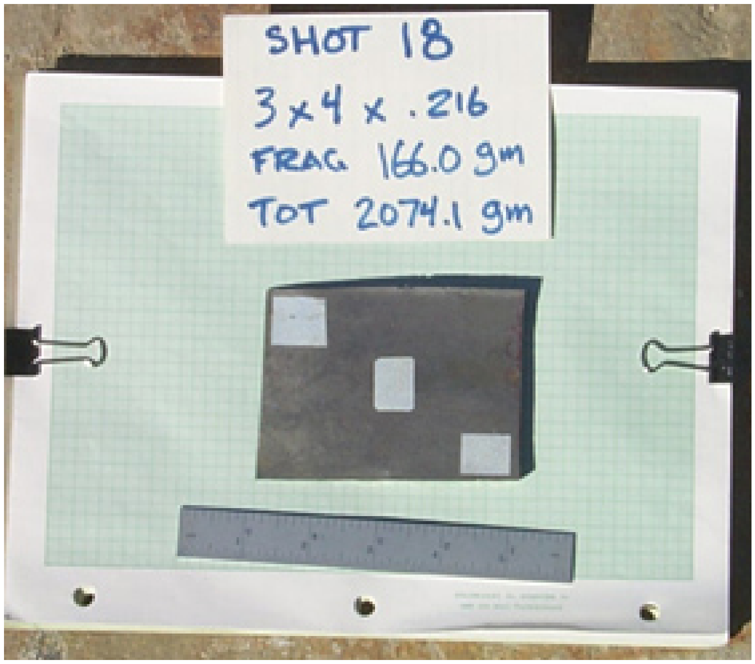

FIGURE 6. SMALL FRAGMENT, 0.67 lb FAN BLADE FRAGMENT

FIGURE 7. DISK FRAGMENT IMPACT, EXTERIOR VIEW

FIGURE 8. LARGE FRAGMENT IMPACT, INTERIOR VIEW

FIGURE 9. BARRIER TEST SHOWING CAPTURED FRAGMENT

FIGURE 10. BARRIER IMPACT SHOWING A PENETRATED INTERIOR WALL PANEL

2.2 TEST PROCEDURE.

The test procedure used for each shot is listed below.

- The fuselage section was rolled and translated to bring the desired target location into the center of the view down the gas gun barrel.
- The backstop position in the fuselage was checked and relocated as necessary to provide for fragment capture.
- The high-speed film cameras' control lines were checked.
- The light control lines were checked.
- The gas gun control lines were checked.
- The camera-to-grid board and camera-to-shotline measurements were made for all cameras.
- The blade fragment was measured and weighed.
- The blade fragment was digitally photographed and placed in the sabot.
- The high-speed film cameras were loaded and armed.

- The sabot with fragment was muzzle-loaded and pushed 10 ft. down the muzzle.
- The test area was cleared of personnel.
- The gas gun was charged with nitrogen to a pressure required for the shot velocity.
- The electronic test sequencer was started and a t-15 second count was begun.
- At t = 0 the fragment was fired.
- Digital images were made of the entrance and exit sides of the fuselage hole.
- The hole was marked for identification.
- The high-speed cameras were unloaded.
- The shot area was cleaned up.

2.3 PRESENTED AREA MEASUREMENT METHODOLOGY.

The following discussion on the methodology to determine the fragment presented area is from reference 1 and presented for completeness. The best method for determining the presented area at impact is to have two high-speed film views of the fragment in flight. For any point in three-dimensional (3D) space, knowing the projected coordinates for any two planes, fully describes the 3D point. Therefore, two cameras set up along orthogonal axes will easily produce corner data from an image that can be transformed into body attitudes. Early in the testing, problems were encountered with locating the two external cameras at right angles. It became clear that the side camera would work, but often the up or down camera would not be locatable, such that the two views would be orthogonal or the aircraft structure and other rigging became obstructions.

Since two views of the fragment in flight was not possible, a technique was needed that would calculate the presented area from one view. Two observations provided the insight into the solution. First, blade fragments usually had very little angular momentum when exiting the sabot stopper. Second, the impact hole geometry provided an indication as to the general orientation of the blade. Projectile corner x,y data (from the side view) was inputted to an Excel spreadsheet model. The model contained a geometric description of the blade based on measurements taken before the shot. After appropriate transformations, the model blade was rotated about the three axes until a best fit to the high-speed film data was obtained. The blade model contained a cambered plate of no thickness. The thickness was input as camber when the camber was smaller than the thickness. The process was automated by using the Excel Solver tool. The Solver tool was allowed to vary all three rotation angles. The goal was to minimize the sum of the root sum squared errors between the model blade and the film data corner locations.

The procedure was scrutinized for every shot. Because the physical situation was fairly well understood, it was possible to quickly spot situations where the method had failed to find the applicable solution. When the solution was incorrect, typically, the roll angle would have the wrong sign. Using the launch attitude as a first guess for the optimizer usually produced the best fit. Figures 11 through 14 are reference frames used in the Excel Solver.

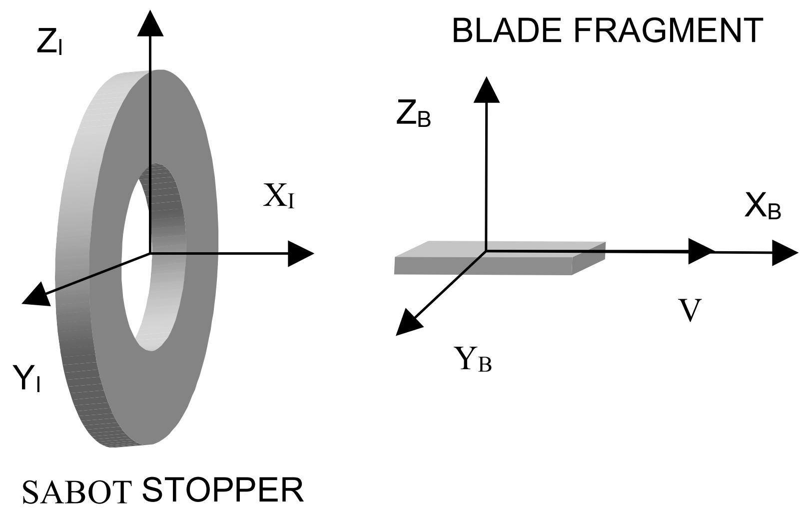

FIGURE 11. LEFT HAND REFERENCE FRAME

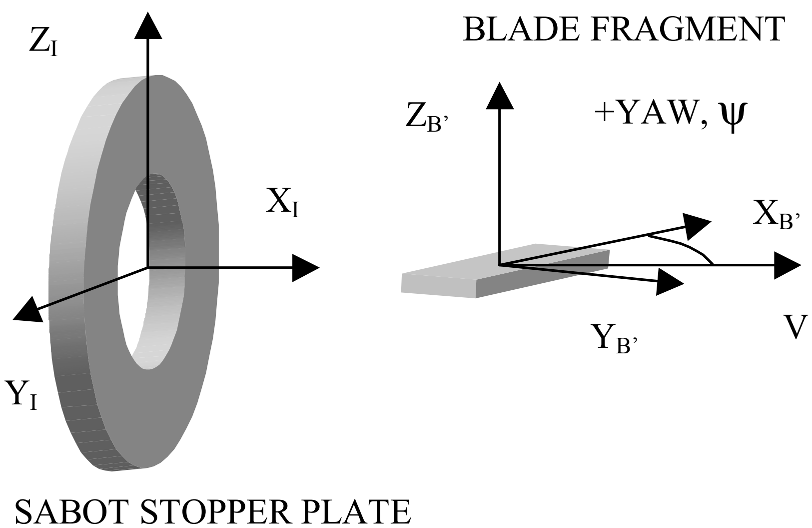

FIGURE 12. FRAGMENT YAW DEFINITION

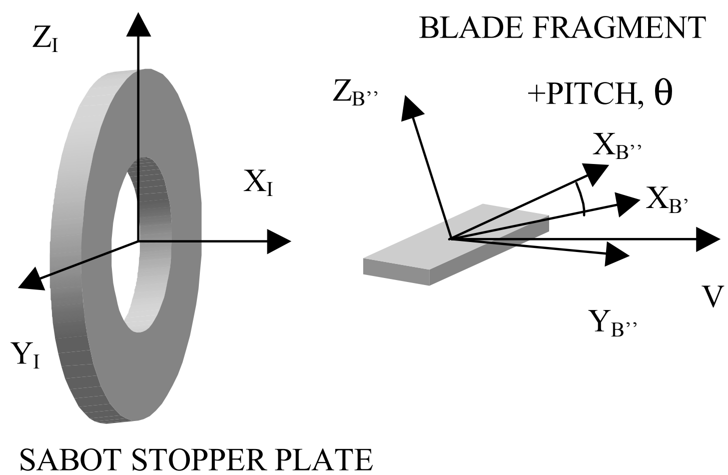

FIGURE 13. FRAGMENT PITCH DEFINITION

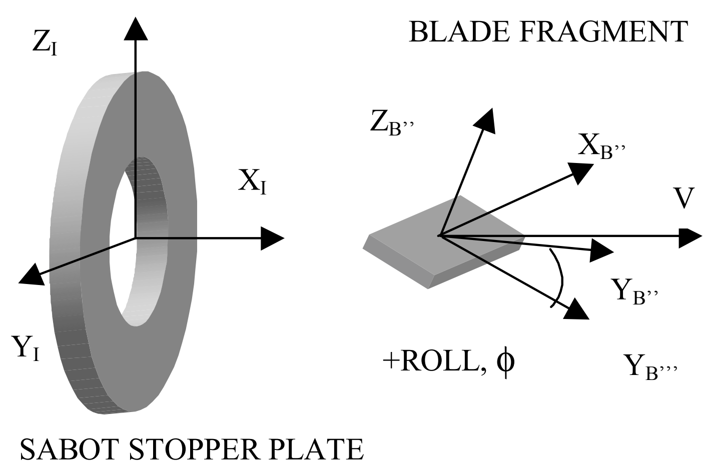

FIGURE 14. FRAGMENT ROLL DEFINITION

2.4 TEST RESULTS.

2.4.1 Analysis Discussion.

The measurement of projectile presented area and presented area perimeter is the most difficult parameter to extract from the experimental data. During the analysis work of Phase I, a software tool was developed to compute the presented area of a projectile from high-speed film data. The impact velocity was calculated by measuring the centroid motion of the fragment image on the film and making scale corrections. The penetration equations were implemented in an Excel spreadsheet. The input data required for the computations of residual velocity are shown in table 3.

TABLE 3. PENETRATION EQUATIONS INPUT PARAMETERS

Parameter
Fragment width
Fragment height
Fragment weight
Release velocity
Obliquity angle
Number of plates
Plate thickness for each plate
Fragment angle for each plate
Material type for each plate

For these tests, all of the parameters could be measured directly except for the fragment impact angle. The penetration equations do not model the impact in 3D. They model the impact as a two-dimensional (2D) impact with an obliquity and an impact angle. The 3D measured presented area was used to calculate the 2D fragment angle for the penetration equations. For each shot, a fragment angle was found that produced the presented area obtained from the high-speed film analysis.

The analysis for the Phase II data started with the same method used on the Phase I data. That method considers the secondary structure, rib or stringer, to be a second plate. Note, the model only allows plates. This produced a nice fit for the data from Phase I. The data for Phase II did not produce a good comparison between experimental and empirical numbers, see section 2.4.2.3. This led to an investigation of alternatives to the simple plate model. During this investigation, it was found that the secondary structure was not contributing significantly to a reduction in residual energies. It was then decided to make a comparison for all the previous data collected (including Phase I) and ignore the secondary structure. This produced a better correlation. Two formulae were used for computing the parameter V_{50}: the JTCG/ME form from the THOR equations, and from reference 4, the FAA V_{50} equation. The difference between the two is that the THOR form uses the presented area and the FAA form uses the perimeter of the presented area. Since large fragments often have large impact perimeters, it was desirable to know if the FAA form would produce a better correlation. The best correlation was obtained with the FAA V_{50} equation and the JTCG/ME form of the residual velocity equation discussed in section 1.2.2.

2.4.2 Results.

During the analysis, it was found that the secondary structure did not play an important role in energy reduction during an aircraft penetration. This result is remarkable and clearly will not apply to very heavy or strong secondary structures like armor. These results are only valid for the types of structures found in a commercial aircraft cabin wall. Figure 15 shows typical secondary structural elements in a typical cabin wall. There are frames in the vicinity of the exit doors that are capable of stopping a 300 gm fragment traveling at 718 ft/s. The data analysis shown in this section indicates that, for all but a few impacts, the secondary structure is not significantly affecting the fragment residual velocities. The experimental data show that the large fragments, which usually strike a portion of a secondary structure, were not greatly affected by that secondary structure.

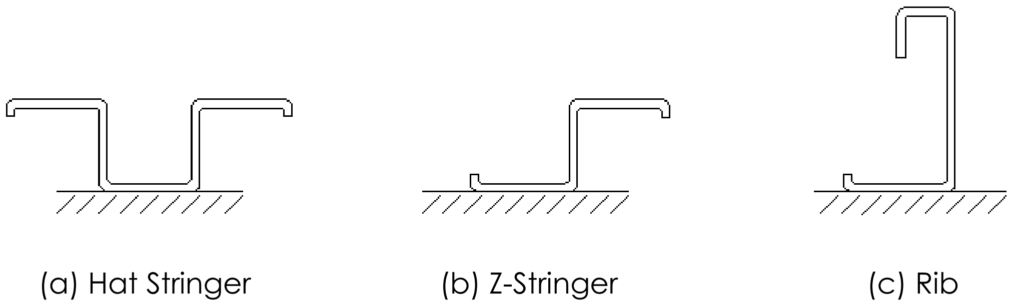

FIGURE 15. TYPICAL STRUCTURAL ELEMENTS

The hat stringers were the widest secondary structures tested. These stringers are approximatley 3 inches wide and did not absorb much energy during impact. Because there was concern about testing mostly smaller fragments in previous tests, all the data collected to date was analysed using the new penetration model.

The normalized velocity, V_n, is used to compare the test results to the penetration models.

$$V_n = 1 - \left(\frac{V_{r_{ACT}} - V_{r_{calc}}}{V_{init}} \right) \tag{3}$$

where:

$V_{r_{ACT}}$ = the actual residual velocity measured during the test
$V_{r_{calc}}$ = the calculated residual velocity from the model
V_{init} = the actual initial velocity measured during the test

With this parameter, the perfect fit of experimental to empirical data would be seen as a plot with all columns standing at exactly 1 unit. Figures 16 through 22 show the results of this comparison.

It should be noted that several other methods were attempted that portioned out the amount of interaction between the projectile and the secondary structure. These were much more complex and proved to be less accurate than any of the three presented here. That work is documented in appendix B. One form considered was the JTCG (and similar THOR) petaling (material failure) form of the residual velocity equation. That method is not applicable to large fragments impacting a structure and did not produce an acceptable correlation.

2.4.2.1 Test 1 [6] Comparison.

Figures 16 and 17 show the results of test 1 of reference 6. All shots in test 1 were skin only. In this test, the correlation to the previous model was not very good.

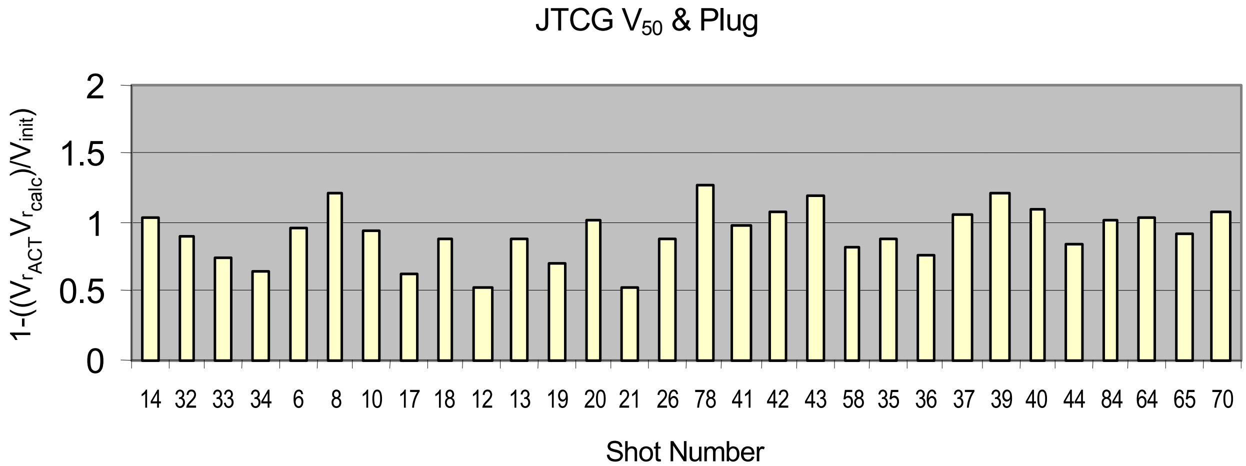

FIGURE 16. TEST 1 [6] RESULTS, JTCG EQUATIONS FOR V_{50} AND V_r USED

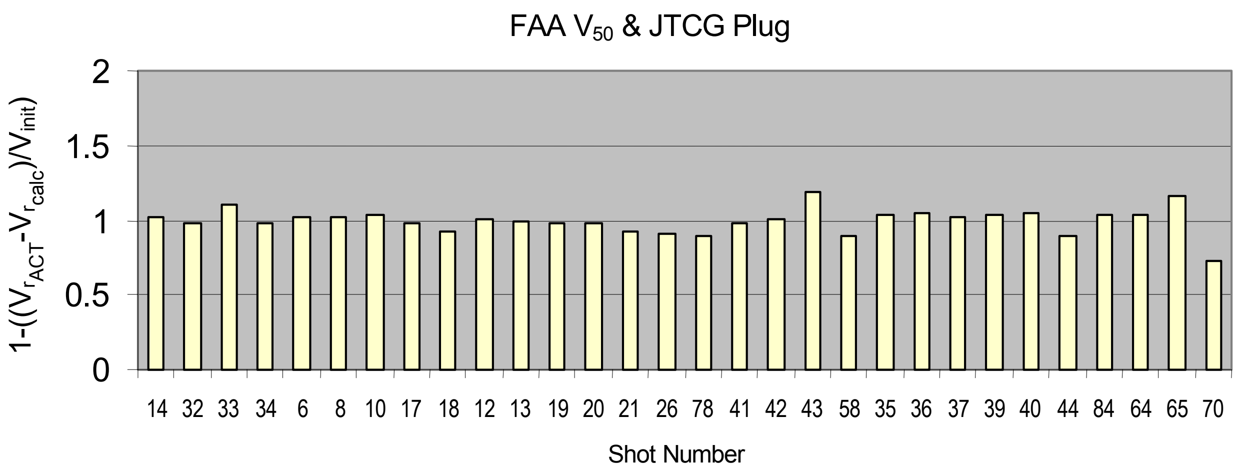

FIGURE 17. TEST 1 [6] RESULTS, FAA EQUATION FOR V_{50} AND JTCG V_r EQUATION USED

2.4.2.2 Test 2 Phase I Comparison

Figures 18 and 19 show results of test 2 of Phase 1 [1]. The results show a better correlation between this improved model over the original model shown in figures 16 and 17.

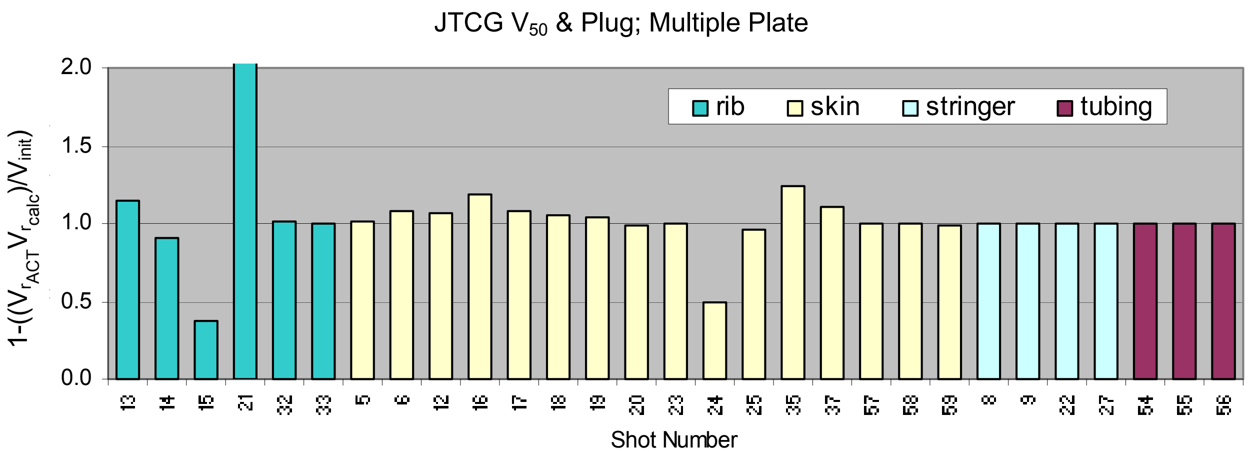

FIGURE 18. JTCG EQUATIONS WITH OTHER STRUCTURE MODELED AS SECOND PLATE

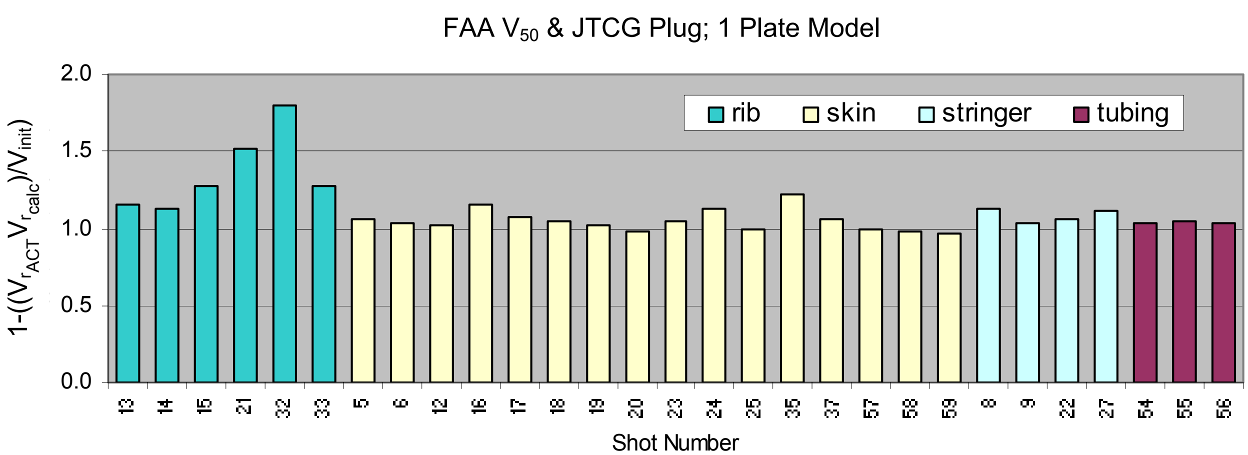

FIGURE 19. FAA V_{50} EQUATION WITH JTCG V_r PLUGGING EQUATION AND NO SECONDARY STRUCTURE MODELING (Single plate model)

2.4.2.3 TEST 2 PHASE II.

The following plots show the results of the data comparisons for Phase II. Figures 20 and 21 show the first attempts at correlating the experimental data with the improved empirical model. They do not show good correlation. This was considered unacceptable and therefore a better model was sought.

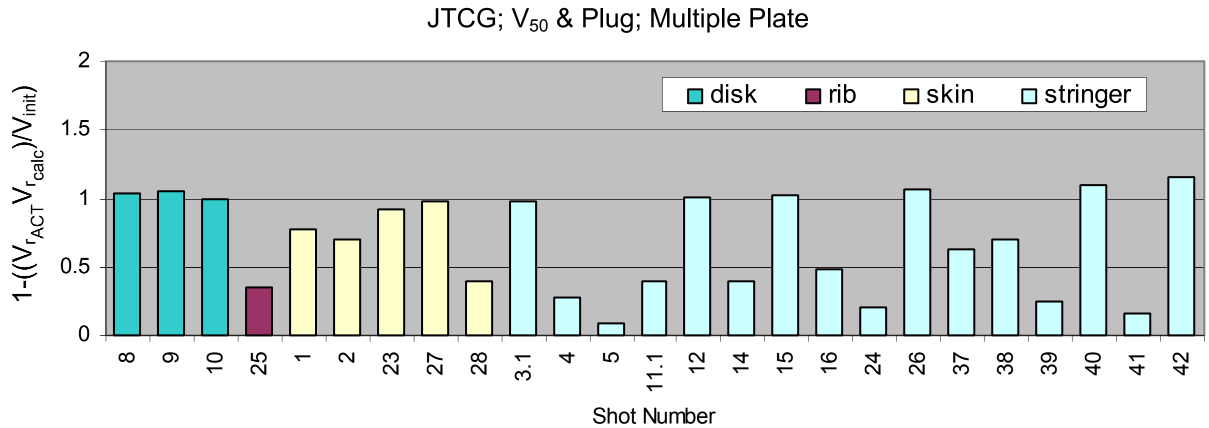

FIGURE 20. JTCG EQUATIONS WITH SECONDARY STRUCTURE MODELED AS SECOND PLATE

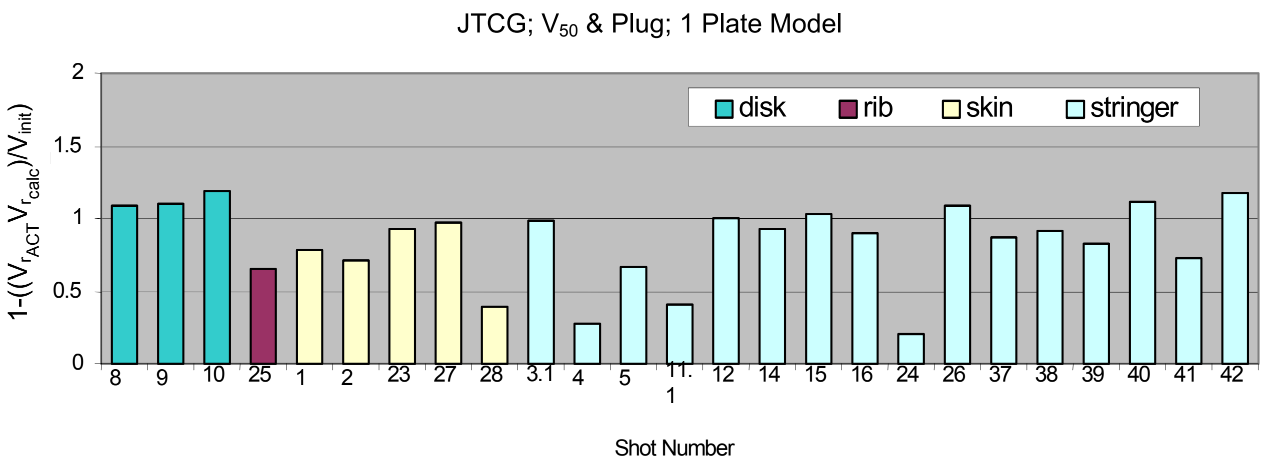

FIGURE 21. JTCG EQUATIONS WITHOUT SECONDARY STRUCTURE

Figure 22 shows the results of the final model. Using the FAA equation for V_{50} and the plugging (material failure) form of the JTCG penetration equations provided a very good model for rapid assessments of shotlines. The secondary structures are not considered in the following plot. Only the skin impact is computed. The experimental data show that for large fragments that strike a protion of a secondary structure, the residual velocity is not greatly affected by that secondary structure. For an 8-inch-wide fragment, even a hat stringer at 3 inches wide does not significantly affect the fragment residual velocity.

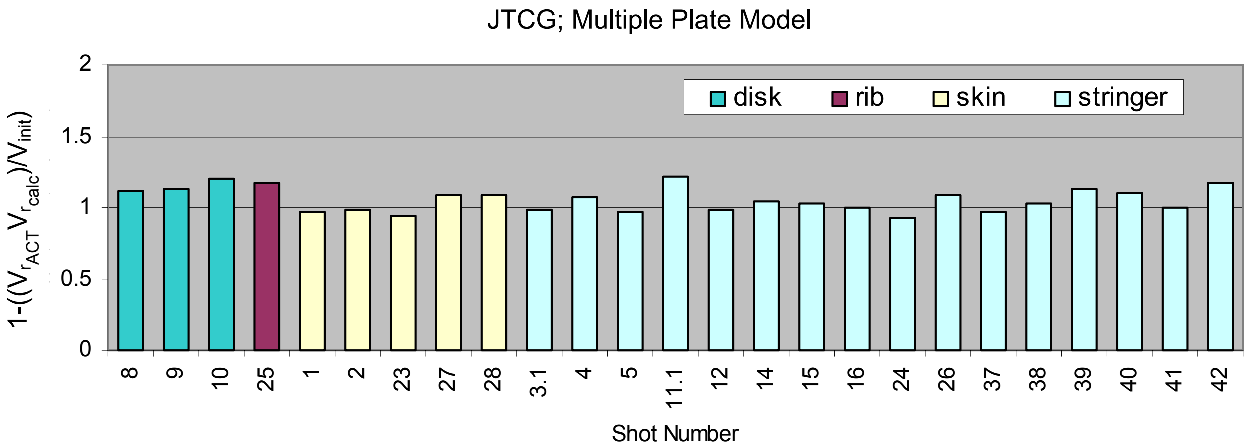

FIGURE 22. FAA V_{50} EQUATION WITH JTCG V_r PLUGGING EQUATION AND NO SECONDARY STRUCTURE MODELING (Multiple plate model)

2.5 SUMMARY.

The Phase II tests were intended to expand existing airframe fuselage test data to include large engine fragments. When the large fragments were used, the aircraft secondary structure (rib or stringer) was also penetrated.

The results of this testing show that the secondary structures are not significant energy absorbers when a small to large fragment impacts an aircraft structure. Additionally, this study indicated that when estimating impact $V_{50,}$ the term perimeter of the fragment presented area is a very important term.

As the fragment size grows the probability of impacting secondary structure grows. An 8- by 8-in. fragment will almost always impact a stringer or rib. The secondary structure usually will only subtend a portion of the 8- by 8-in. fragment. It is a surprising result that the secondary structure does not cause a significant drop in fragment energy. As the analysis method became more complex in an attempt to model the secondary structure, there was less agreement with the results. It was that observation that suggested running a simple correlation using a single-plate model that used only the skin parameters. When the 8- by 8-in. data showed favorable agreement with the test data, all previous data collected to date was correlated in the same manner. In all cases, the single-plate model shows the best correlation to the experimental results.

It was expected that a measurable delta in residual energy would be seen due to the impact of a secondary structure, especially when the secondary structure was completely severed or broken away. Reference 9 suggests that there may be an effect due to the propagation of stress waves that may be weakening the secondary structure. A stress wave propagates at velocities from 15,000-25,000 ft/s and may arrive at the secondary structure from 4-64µs prior to the fragment's arrival. Previous work, as indicated in reference 9, has measured significant changes in a material's stress-strain relationship due to stress waves. It cannot be said that this effect is a major one in the test since there was no attempt to measure the strength of the propagated waves.

Another possibility for not measuring appreciable energy drops is due to indeterminate and systematic experimental errors. These are due, in part, to the blur in the images, fragments being broken at launch and not matching the model exactly, and the model of the fragments not being an exact cambered, tapered, nonrectangular model. Based on the known errors, a 10%-15% sigma is likely.

Based on all the work done to date a simple method of estimating residual energies for turbine engine fragments has been found. That methodology is to use the FAA V_{50} equation and the THOR residual velocity equation.

2.6 FUTURE PLANS.

This method of analysis has been shown to be very good for aluminum structures, but there are no V_{50} values available for composite structures. With ever increasing use of composite structures, the next phase of this program will be expanded to cover composite materials. This is a complex problem due to the varied use of composites. Aluminum structures tend to be very similar, while composite structures are very different in terms of mechanical layout. As a first cut, even some simple tests to measure the V_{50}'s for some simple composite panels would be very useful. It is planned to develop at least one V_{50} for a composite panel that might be acceptable to the industry as a test standard. There is a lack of data for titanium as well, and it is planned, for the same reasons as above, that some titanium impacts be made to evaluate V_{50}. During the course of V_{50} measurements, some penetration should occur. This data can be used to determine a value for the dynamic shear strength of the material by curve fit techniques.

In addition, to expand the data in the design of shields for aircraft structures, it is planned to conduct multiple-plate tests. It is planned to conduct a few tests of multiple thick plates of aluminum and steel to evaluate the applicability of this methodology to shield design.

3. REFERENCES.

1. Lundin, S., "Engine Debris Fuselage Penetration Testing Phase I," DOT/FAA/AR-01/27, August 2001.

2. "The Resistance of Various Metallic Materials to Perforation by Steel Fragments," Ballistic Analysis Laboratory, Johns-Hopkins University, Baltimore, MD, BAL, April 1963, THOR TR No. 51, Confidential.

3. "Penetration Equations Handbook for Kinetic-Energy Penetrators" (U), Joint Technical Coordinating Group for Munitions Effectiveness (Anti-Air), 15 October 1985, 61 JTCG/ME-77-16, Revision 1.

4. Gunderson, C., Study to Improve Airframe Turbine Engine Rotor Blade Containment, McDonnell Douglas Corp, FAA report RD-77-44, July, 1977.

5. "Standard Test Method for Dynamic Young's Modulus, Shear Modulus, and Poisson's Ratio by Impulse Excitation of Vibration," American Society for Testing and Materials, March 1999, E1876-99, www.astm.org.

6. Manchor, J. and Frankenberger, C., “Engine Debris Penetration Testing,” DOT/FAA/AR-99/19, June 1999

7. Erlich, D.C., Shockey, D.A., and Simons, J.W., “Full-Scale Tests of Lightweight Fragment Barriers on Commercial Aircraft”, SRI International, DOT/FAA/AR-99/71, November 1999

8. Erlich, D.C., Shockey, D.A., and Simons, J.W., “Improved Barriers to Turbine Engine Fragments: Interim Report IV;” DOT/FAA/AR-99/8, IV, June 2002

9. Kolsky, H., “Stress Waves in Solids,” Dover Publications, NY, NY, 1963.

APPENDIX A—DIMENSIONAL ANALYSIS OF PENETRATION EQAUTIONS

The following is a dimensional check of the units associated with the penetration model selected from this testing.

Parameters:

L = Presented area perimeter (m)
A_p = Presented area (m^2)
G_d = Dynamic Shear Modulus (Pa)
t = Target thickness (m)
m = Mass of fragment (kg)
θ = Obliquity of impact (deg; 90° is edge on)
ρ = Density of the target material (kg/m^3)
V = Impact velocity
V_r = Residual velocity
V_{50} = Velocity for which 50% of the fragments will penetrate

FAA V_{50} Equation:

$$V_{50} = \sqrt{\frac{2 \cdot L \cdot G_d \cdot t^2}{m \cdot \cos^2 \theta}}$$

$$V_{50} = \left(\frac{m * Pa * m^2}{kg}\right)^{\frac{1}{2}} = \left(\frac{m^3 * \frac{N}{m^2}}{kg}\right)^{\frac{1}{2}} = \left(\frac{N * m}{kg}\right)^{\frac{1}{2}} = \left(\frac{\frac{kg * m}{s^2} * m}{kg}\right)^{\frac{1}{2}} = \left(\frac{m^2}{s^2}\right)^{\frac{1}{2}} = \frac{m}{s}$$

JTCG/AS Residual Velocity Equation:

$$V_r = \frac{\sqrt{V^2 - V_{50}{}^2}}{1 + \frac{\rho \cdot A_p \cdot t}{m \cdot \cos(\theta)}}$$

$$V_r = \frac{\left(\frac{m}{s}\right)^{\frac{1}{2}}}{\frac{\frac{kg}{m^3} * m^2 * m}{kg}} = \frac{m}{s}$$

APPENDIX B—A STUDY OF IMPROVEMENTS TO THE EXISTING PENETRATION EQUATIONS TO INCLUDE THE EFFECTS OF STRUCTURAL ELEMENTS

NAWCWD TM 8339

A Study of Improvements to the Existing Penetration Equations to Include the Effects of Structural Elements

by
Richard B. Mueller

APRIL 2002

NAVAL AIR WARFARE CENTER WEAPONS DIVISION
China Lake, CA 93555-6100

FOREWORD

This report documents the results of a study conducted to improve the software code used in the Uncontrolled Debris Model (UDM). The UDM is used to predict the residual velocity of the impactor with the interaction of aircraft structural elements. This study was performed by the Naval Air Warfare Center Weapons Division, Systems Vulnerability Branch and funded by the Department of Transportation, Federal Aviation Administration Catastrophic Failure Prevention Program, through the FAA Technical Center, Atlantic City International Airport, New Jersey.

The report was reviewed by Charles Frankenberger and Steve Lundin. The findings of this study are preliminary in nature, and the report is released at the working level.

R. A. HORTON, Head
Survivability Division
Research and Engineering Department
15 April 2002

NAWCWD TM 8339, published by Technical Information Division, 1 electronic copy.

NAWCWD TM 8339

A Study of Improvements to the Existing Penetration Equations to Include the Effects of Structural Elements

This document has been reviewed and approved for publication by:

REVIEWED BY: DATE

3/8/02

Charles Frankenberger
Project Engineer
Code 418300D

3/11/02

Steve Lundin
Project Engineer
Code 418300D

3/11/02

A. J. Wearner
Head, Systems Engineering Branch,
Code 418300D

APPROVED BY:

4/15/02

Richard (Tim) Horton
Head, Survivability Division
Code 418000FAA

REPORT DOCUMENTATION PAGE	*Form Approved* *OMB No. 0704-0188*

1. AGENCY USE ONLY *(Leave Blank)*	2. REPORT DATE	3. REPORT TYPE AND DATES COVERED
	April 2002	Final

4. TITLE AND SUBTITLE

A Study of Improvements to the Existing Penetration Equations to Include the Effects of Structural Elements (U)

5. FUNDING NUMBERS

6. AUTHOR(S)

Richard B. Mueller

7. PERFORMING ORGANIZATION NAME(S) AND ADDRESS(ES)

Naval Air Warfare Center Weapons Division
China Lake, CA 93555-6100

8. PERFORMING ORGANIZATION REPORT NUMBER

NAWCWD TM 8339

9. SPONSORING/MONITORING AGENCY NAME(S) AND ADDRESS(ES)

10. SPONSORING/MONITORING AGENCY REPORT NUMBER

11. SUPPLEMENTARY NOTES

12a. DISTRIBUTION/AVAILABILITY STATEMENT

A Statement

12b. DISTRIBUTION CODE

13. ABSTRACT (*Maximum 200 words*)

(U) This report documents the results of a study that analyzed potential improvements to the software code used in the Uncontrolled Debris Model (UDM). The study focused on penetration equations in the UDM code that determine the residual velocity of a projectile (impactor) after penetrating an aircraft's surface. The analysis focused on three of the aircraft's structural elements—z-stringer, hat stringer, and rib.

(U) In addition to the UDM code, the Thickness Coefficient Solver and Thickness Coefficient Solver Linear Distribution programs were used as analysis tools. The study looked at results from two different perspectives: the impactor as several smaller fragments, and the impactor as one large fragment.

14. SUBJECT TERMS

Uncontrolled Debris Model; Structural Elements; Penetration Equations; UDM; Thickness Coefficient Solver; Residual Velocity; Engine Fragments

15. NUMBER OF PAGES

47

16. PRICE CODE

17. SECURITY CLASSIFICATION OF REPORT	18. SECURITY CLASSIFICATION OF ABSTRACT	19. SECURITY CLASSIFICATION OF THIS PAGE	20. LIMITATION OF ABSTRACT
UNCLASSIFIED	UNCLASSIFIED	UNCLASSIFIED	SAR

NSN 7540-01-280-5500

Standard Form 298 (Rev. 2-89)
Prescribed by ANSI Std. 239-18
29-102

CONTENTS

Acronyms ... 3

Introduction ... 5

Basic Theory ... 5

Background ... 6

Procedure ... 8
- Solving the Impactor as Several Smaller Fragments ... 9
  - Thickness Coefficient for Entire Width of Structural Element ... 10
  - Thickness Coefficient for Base Width of Structural Element ... 11
  - Thickness Coefficient for Base Width of Structural Element With New Stopping Conditions ... 12
  - Thickness Coefficient for Base Width of Structural Element With Linear Weight Distribution ... 12
- Solving for the Impactor as One Large Fragment ... 12
  - Percentage of Impactor Contacting the Structural Element and the Change in Kinetic Energy ... 13
  - Initial Velocity With Respect to the Change in Kinetic Energy ... 13
  - Presented Area Ratio With Respect to the Prediction Accuracy ... 13

Analysis Tools ... 13
- Uncontrolled Debris Model (Udm) ... 14
- Thickness Coefficient Solver ... 14
  - Testing ... 15
- Thickness Coefficient Solver With Linear Weight Distribution ... 16

Results ... 17
- Solving the Impactor as Several Smaller Fragments ... 17
  - Thickness Coefficient for Entire Width of Structural Element ... 17
  - Thickness Coefficient for Base Width of Structural Element ... 19
  - Thickness Coefficient for Base Width of Structural Element With New Stopping Conditions ... 21
  - Thickness Coefficient for Base Width of Structural Element With a Linear Weight Distribution ... 21
- Solving the Impactor as One Large Fragment ... 23
  - Percentage of Impactor Contacting the Structural Element and the Change in Kinetic Energy ... 24
  - Initial Velocity With Respect to the Change in Kinetic Energy ... 26
  - Presented Area Ratio With Respect to the Prediction Accuracy ... 26

Conclusions ... 28

References 28

Appendixes:
A. Uncontrolled Debris Model 29
B. Thickness Coefficient Solver 35
C. Thickness Coefficient Solver Linear Weight Distribution.......... 45

Figures:

1. Flowchart of the Development Process. 8
2. Smaller Fragment Numbering Scheme. 10
3. Definition of Base and Entire Width for Various Structural Elements 11
4. Comparison of Small Fragment Weight Distribution. 17
5. Thickness Coefficients for Entire Width of Structural Element of All Structural Elements. 18
6. Comparison of Thickness Coefficient for Base Width and Entire Width of Hat Stringer. 19
7. Comparison of Thickness Coefficients for Base Width and Entire Width of Rib. 20
8. Comparison of Thickness Coefficient for Base Width and Entire Width of Z-Stringer. 20
9. Comparison of Thickness Coefficients for Base and Entire Width of All Structural Elements. 21
10. Change in Kinetic Energy for Base Width and Entire Width of Hat Stringer. 24
11. Change in Kinetic Energy for Base Width and Entire Width of Rib. 25
12. Change in Kinetic Energy for Base Width and Entire Width of Z-Stringer. 25
13. Change in Kinetic Energy for Base Width and Entire Width of All Structural Elements. 26
14. Comparison of Initial Velocity to the Change in Kinetic Energy for All Structures 27
15. Comparison of Prediction Accuracy with Respect to Area Ratio. 27

Tables:

1. Summary of Structural Element Impact Test Data 8
2. Structural Element Impact Regions Using Entire Width Criteria 11
3. Structural Element Impact Regions Using Base Width Criteria 12
4. Comparison of Residual Velocities for the UDM and Thickness Coefficient Solver. 16
5. Comparison of Results Between V_{res} and KE_{res} Stopping Conditions for Entire Width 22
6. Comparison of Results Between V_{res} and KE_{res} Stopping Conditions for Base Width. 22
7. Comparison of Results Between Equal and Linear Weight Distribution for Entire Width. 23
8. Comparison of Results Between Equal and Linear Weight Distribution for Base Width 23

ACRONYMS

AAA	Anti-aircraft artillery
JTCG/ME	Joint Technical Coordinating Group for Munitions Effectiveness
KE	Kinetic energy
KE_{res}	Residual kinetic energy
MIKES	Missile Impact Kinetic Energy Simulator
UDM	Uncontrolled Debris Model
V_{res}	Residual velocity

(This page intentionally left blank.)

INTRODUCTION

The objective of this study was to improve the Uncontrolled Debris Model (UDM) code to enable a more accurate prediction of the residual velocity of the impactor with the interaction of aircraft structural elements. The UDM code provides accurate solutions only for fragment impacts against the aircraft's skin. However, the solutions become inaccurate when the impact surface includes a structural element, such as a z-stringer, hat stringer, or rib. The existing penetration equations are simple and the code very short and improvements should consider both of these factors.

BASIC THEORY

The penetration equations are a set of empirically derived equations that determine the residual velocity of a projectile (impactor) after penetrating a surface. These equations were originally defined by the Joint Technical Coordinating Group for Munitions Effectiveness (JTCG/ME), to predict the result of antiaircraft artillery (AAA) projectiles and their shrapnel fragments against aircraft. The penetration equations are stated in numerous forms that are determined by (1) whether or not the projectile (or fragments of shrapnel) plug or petal the surface, and (2) the breakup of an incendiary projectile's core.

The penetration equations used in the UDM code are derived from the equations for a fragment that plugs the impacted surface. A plug occurs when the projectile penetrates a surface by removing a piece of the surface approximately the same area as the contact area of the impactor. The effective presented area (A_p) is the actual area of the impactor that contacts the surface and is written as

$$A_p = \cos(\theta) \bullet w \bullet d$$

where w is the width of the fragment, d is the length of the fragment, and θ is the obliquity angle. The obliquity angle is defined as the angle between the surface of the fragment and a line perpendicular to the shot line.

The penetration equations also contain several dimensionless constants, denoted as Q_n, for example

$$Q_8 = \frac{1980 \bullet t \bullet A_p}{Wt}$$

$$Q_{11} = \frac{Q_8 \bullet Wt}{100}$$

These constants are a function of weight (Wt) and the thickness of the impacted surface (t). In the following equation, the ballistic limit (V_{50}) determines if the impactor has enough energy to penetrate the surface, and is described as follows:

$$V_{50} = 3.2808399 \bullet C_{bf} \bullet Q_8^{bf} \bullet \left(\frac{1}{\cos(\theta)} \right)^h Q_{11}^f$$

where C_{bf}, h, f, and bf are empirical constants.

The residual velocity (V_{res})is solved by first defining another dimensionless constant, Q_4.

$$Q_4 = \frac{\rho \bullet A_p \bullet t}{Wt \bullet \cos(\theta)}$$

$$V_{res} = \frac{\sqrt{\left(V_0^2 - V_{50}^2\right)}}{\left(1 + Q_4\right)}$$

where ρ is the density of the material being impacted. The residual kinetic energy can be determined from the residual velocity.

BACKGROUND

UDM code improvements were considered from two separate approaches—one analytical, and one empirical. The analytical approach would use advanced beam theory and other structural analysis tools to determine a solution while the empirical method would take actual test data and attempt to find an equation to describe these results. The analytical approach would be an extremely complex task to write in code. Because non-adiabatic conditions exist throughout the system (impactor and impacted surface), which could prevent the solution from providing accurate data, the empirical was determined to be the best approach. Also, the existing analysis tool, the UDM program, was written with equations developed from empirical data by the JTCG/ME.

The object of the empirical approach is to find a relationship or characteristic to describe test data. The data used for this analysis is from Phase I of the Engine Debris Penetration Testing performed in September 1999 by the Naval Air Warfare Center, Weapons Division, China Lake (Reference 1). Of the 64 impact tests performed, only 22 involved a structural element. Also, because of either a shot (impact) failure or missing data, only 10 of these tests were viable for use as analysis data (see Table 1). The tests included three types of structural elements: three z-stringers, four rib, and three hat stringers.

The test data came in three forms.

1. Shot test data sheets, including MIKES setup and high-speed camera analysis.
2. Digital camera files of the impact area for qualitative analysis.
3. Post test UDM analysis.

Initial observation of the test data and comparison of the residual velocities with results from the UDM code showed that the three structural types had different effects on the residual velocity.

TABLE 1. Summary of Structural Element Impact Test Data.

Shot	Structural component	Viable data	Comments
4	Z-Stringer	Yes	
7	Z-Stringer	No	Shot data is incomplete
8	Z-Stringer	Yes	
9	Z-Stringer	Yes	
10	Hat Stringer	No	Shot data is incomplete
11	Hat Stringer	Yes	
13	Rib	Yes	
14	Rib	Yes	
15	Rib	Yes	
21	Rib	Yes	
22	Hat Stringer	Yes	
26	Hat Stringer	No	Shot failure*
26B	Hat Stringer	Yes	
27	Hat Stringer	No	Shot failure*
28	Rib	No	Shot data is incomplete
28B	Rib	No	Shot failure*
29	Rib	No	Shot failure*
30	Rib	No	Shot failure*
31	Rib	No	Impacted bulkhead
32	Rib	Yes	
34	Rib	No	No pictures available
36	Z-Stringer	No	Picture is unclear

*Due to sabot, high-speed camera, or lighting malfunction.

PROCEDURE

Two distinct categories of analysis were used in the development of an empirical tool to describe the effects of structural elements. The first was to break the large fragment in several smaller fragments to be resolved individually. The data from the smaller pieces was then averaged into one solution for a large fragment. In the second, the large fragment is kept as one piece. The entire development process can be divided into two approaches with six distinct stages.

1. Solving the impactor as several smaller fragments by looking at
   a. A thickness coefficient for the entire width of the structural element.
   b. A thickness coefficient for the base width of the structural element using Vres stopping conditions.
   c. A thickness coefficient for the base width of the structural element using KEres stopping conditions.
   d. A thickness coefficient for the base width of the structural element using a linear distribution of weight.
2. Solving the impactor as one large fragment by comparing
   a. The change in kinetic energy.
   b. The prediction accuracy.

Figure 1 shows this development process in a flowchart. The two approaches are explained further in the following sections.

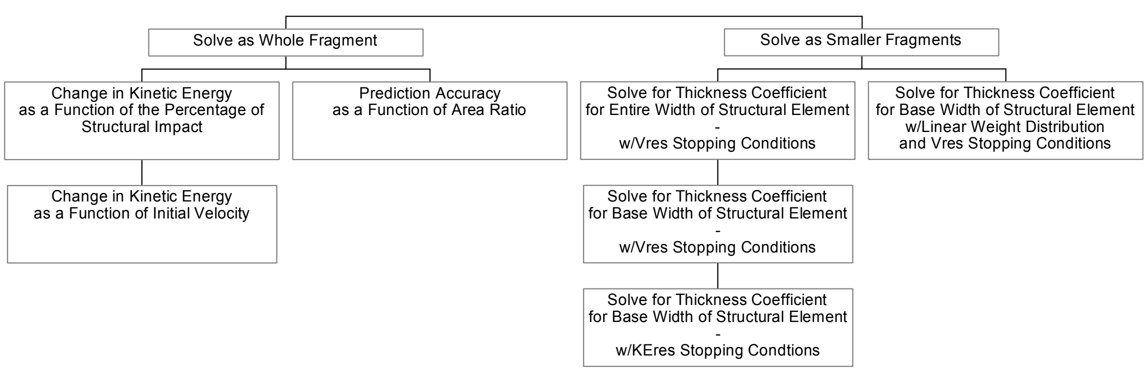

FIGURE 1. Flowchart of the Development Process.

SOLVING THE IMPACTOR AS SEVERAL SMALLER FRAGMENTS

The general concept of this approach was that large impactor fragments should be broken up into several smaller ones, and evaluated individually. Only those smaller fragments that impacted a structural element should have the additional thickness included in the penetration equations. To obtain a realistic solution, the smaller impactor fragment solutions must be reconstructed to provide an effective solution for the larger fragment. For example, if a large impactor fragment is broken into three sections, the center section impacts both the skin and a structural element, and the outer sections impact only the skin. The solution would not be very realistic to say that the outer sections penetrated and the center section did not if the impactor had actually penetrated. This same unrealistic solution would also provide a poor analysis of further impacts that the fragment may encounter.

The UDM code was modified to break up the large fragment into several smaller fragments of equal weight and size, and allow the user to specify which fragments contacted structural elements. The experimental value for the impactor residual velocity was also entered into the program, and the code set to solve for a multiple of the structural element’s thickness to obtain that velocity. In this modified form the code is called the Thickness Coefficient Solver. A further modification of the UDM code broke the large fragment into smaller fragments of equal size but of different weights. The weight distribution was biased toward the center fragments. This code is the Thickness Coefficient Solver Linear Weight Distribution. These codes are described in more detail in the Analysis Tools section.

Two major assumptions were made for this analysis: (1) the large fragment is broken into 10 smaller fragments and (2) the impactor was at a pitch angle of zero at the time of impact. The impactor was broken into 10 smaller fragments. Though arbitrarily chosen, this number of fragments allowed the impactor to be easily sectioned into 10% segments. Any number of sections could easily be added to the code. The smaller fragments were numbered 1 to 10 from top to bottom, shown in Figure 2. The accuracy of determining the percentage location of the structural element from photographs of previous testing was (at best) approximately within + or - 5%.

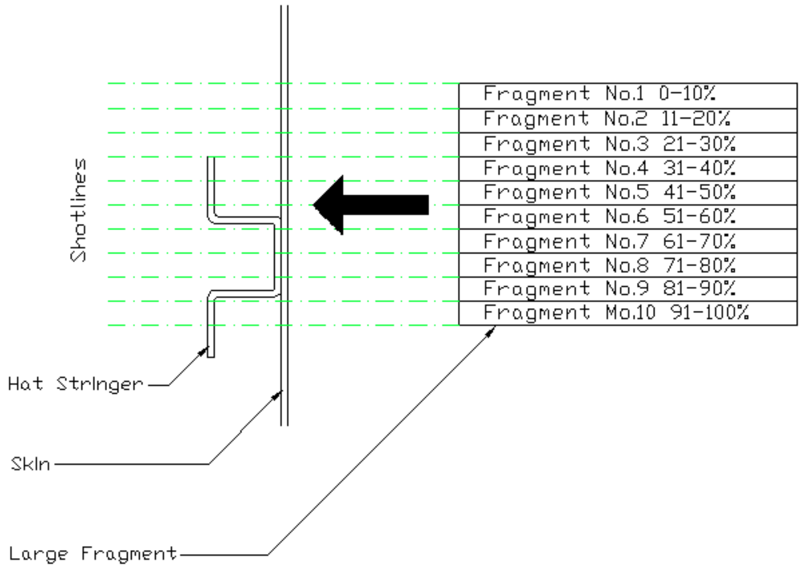

FIGURE 2. Smaller Fragment Numbering Scheme.

The pitch angle of the impactor was assumed to be zero at the point of impact because the pitch angle from most of the testing was less than 10°. The pitch angle of the impactor was not accounted for in the original UDM program.

Thickness Coefficient for Entire Width of Structural Element

The first attempt at establishing a relationship for the effect of structural components considered the entire width of the structural element. The entire width includes those parts of the rib or stringer that are not in direct contact with the skin, but are in the path of the impactor's shot line. Figure 3 shows how the entire width was defined for the three structural types encountered in this study. In the Thickness Coefficient Solver input fields, those fragments that impacted both the skin and the structural component are noted as having two plates.

The analysis was performed with data from 11 test shots. The digital camera photos of each shot were reviewed and the region of the large fragment that impacted the structural element was noted. Table 2 lists the location on the large fragment that impacted a structural component. The Thickness Coefficient Solver code was run with the listed input conditions and the results were plotted.

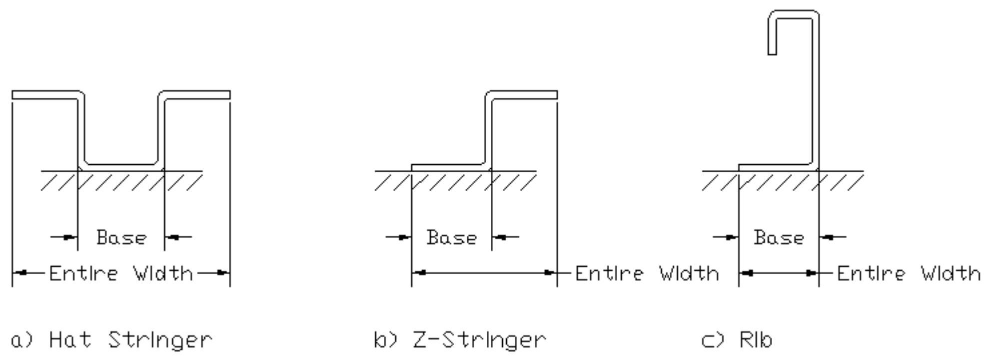

FIGURE 3. Definition of Base and Entire Width for Various Structural Elements.

TABLE 2. Structural Element Impact Regions Using Entire Width Criteria.

Shot	Structural component	Impact location of structural component	
		Beginning, %	Ending, %
4	Z-Stringer	90	100
8	Z-Stringer	0	50
9	Z-Stringer	0	50
11	Hat Stringer	0	30
13	Rib	0	70
14	Rib	0	100
15	Rib	0	100
21	Rib	0	10
22	Hat Stringer	0	90
26B	Hat Stringer	0	80
32	Rib	50	100

Thickness Coefficient for Base Width of Structural Element

The same 11 test shots were again run in the Thickness Coefficient Solver but this time using the base width (see Figure 3) as the structural impact region. Visual analysis of the digital camera pictures determined the structural impact regions on the large fragment. The data is listed in Table 3.

TABLE 3. Structural Element Impact Regions Using Base Width Criteria.

Shot	Structural component	Impact location of structural component	
		Beginning, %	Ending, %
4	Z-Stringer	-	-
8	Z-Stringer	20	50
9	Z-Stringer	10	50
11	Hat Stringer	10	30
13	Rib	30	100
14	Rib	0	100
15	Rib	0	100
21	Rib	0	10
22	Hat Stringer	20	50
26B	Hat Stringer	20	60
32	Rib	50	100

Thickness Coefficient for Base Width of Structural Element with New Stopping Conditions

This study was a repeat of the previous, but with a temporary modification to the Thickness Coefficient Solver code to use KE_{res} instead of V_{res} as the stopping criteria. The new stopping conditions were incorporated in an attempt to reduce the number of data points where the code was unable to provide a solution. The input was also the same as the previous study.

Thickness Coefficient for Base Width of Structural Element with Linear Weight Distribution

A new code, the Thickness Coefficient Solver with Linear Weight Distribution, was written to vary the weight of the smaller fragments. This study was performed to determine if there was any effect based on the proximity of the structural element to the impactor's center of mass. As in the two proceeding cases, the study used the base width of the structural element.

SOLVING FOR THE IMPACTOR AS ONE LARGE FRAGMENT

This aspect of the study was an alternative approach to the multiple fragments when it was determined that no clear solution was obtained using that method. This analysis did not use any special analytical tools, but instead concentrated on plotting the test data to look for a relationship.

Percentage of Impactor Contacting the Structural Element and the Change in Kinetic Energy

In this study, the percentage of impactor that contacted a structural element was plotted against the change in kinetic energy of the impactor. The base width and entire width criteria were studied.

Initial Velocity with Respect to the Change in Kinetic Energy

The initial velocity of the fragment was plotted against the change in kinetic energy of the fragment. This analysis was performed in a continuing attempt to ascertain trends.

Presented Area Ratio with Respect to the Prediction Accuracy

The prediction accuracy was plotted against the area ratio to determine which particular shots were not well predicted by the UDM. This approach was previously used in Reference 1. The prediction accuracy and area ratio were defined as follows:

$$Prediction\ Accuracy = 1 - \left(\frac{V_{res\exp} - V_{resUDM}}{V_0} \right)$$

$$Area\ \_\ Ratio = \frac{A_p}{A_{Total}} = \frac{\cos(\theta) \bullet w \bullet d}{w \bullet d}$$

The area ratio does not include any thickness for the impactor. However, thickness of the impactor was never included in the UDM program.

Those shots where the prediction accuracy was less than 0.8 or greater than 1.2 were then scrutinized for anomalies.

ANALYSIS TOOLS

Three major analysis tools were used in the overall effort to improve the UDM code: the UDM, and the Thickness Coefficient Solver, and Thickness Coefficient Solver Linear Distribution programs. The two programs are modifications of the former UDM code. These new codes were designed for entering and analyzing data with the greatest possible efficiency. The spreadsheet input regions were arranged so test data could be entered in the same order that they were read from the test data sheets. The code was customized to iterate through certain variables until a solution duplicated the test data.

UNCONTROLLED DEBRIS MODEL (UDM)

This debris analysis program has been used for several engine debris studies. The code was written around the JTCG/ME penetration equations for the ballistic prediction of warhead fragments. The effects of these warhead fragments are representative of engine debris. The code and spreadsheet for the UDM are included as Appendix A.

THICKNESS COEFFICIENT SOLVER

The purpose of this program is to calculate a thickness coefficient that would produce a residual velocity within 2% of the actual residual velocity from a test. For example, if the thickness of the material used to form a z-stringer is 0.036"; what multiple of this thickness would represent the z-stringer as a flat plate?

Both the spreadsheet and the code were modified from the existing debris analysis program. Modifications to the spreadsheet were

1. The creation of four separate input regions
    - Impactor Global Specifications
    - Impactor Local Specifications
    - Impacted Surface Data
    - Experimental Results
2. Modification of the output section
3. Creation of the optimizer loop with real-time display

The code and spreadsheet for the Thickness Coefficient Solver are included as Appendix B. The four input regions were created to simplify the data entry process by separating the inputs into categories. The inputs in the Impactor Global Specifications region are the same as the original program, but with the addition of a field for the shot number. Furthermore, the input field for *weight* has been simplified from the original program, which required the entry to be made in grams and multiplied by another cell. The new field requires only that the entry be made in grams, with the conversion from grams to grains and pound force (lbf) now performed within the program. Grams were selected as the units for weight because all data from actual testing gave the impactor weights in grams.

The Impactor Local Specifications region is an addition to the original program. This section has 10 input fields, one for each section of the impactor fragment. These fields state whether the fragment impacted skin only (Field Value=1) or whether a structural element was involved (Field Value=2). The values of one and two are derived from the UDM code where the number of plates impacted would be entered. Skin is only one plate, while skin and structure would be two plates.

The Impacted Surface Data region is where the thickness of the surface (skin and/or structural element) is entered. These fields were in the previous program, but displayed differently.

The Experimental Results region has one field to enter the residual velocity obtained from experimental data. This field was not in the original program, and serves as the stopping criteria for the thickness solver loop.

The output data section provides the same details as the original program, but in a different format. Each small fragment is listed separately. The totals for each output item are placed below each column. These are either mean averages or summations and are described in more detail in the code description section.

This program was designed to find a solution for the thickness coefficient. An additional region was placed on the spreadsheet that gave a real-time display of (1) the number of iterations, (2) the value of the thickness coefficient, and (3) the percentage difference between calculated and experimental residual velocities. This allowed the user to see whether the program was converging on or diverging from a solution.

The Visual BASIC code for the Thickness Coefficient Solver program differed from the original penetration equations program in that it broke the fragment into ten equally sized parts across the width. Weight and width were the only parameters that needed to be divided by 10. The code iterated through penetration equations for each of the smaller fragments until the stopping criteria was met. Data is output for both the whole fragment and each of the smaller fragments.

The code was modified to break the large fragment into 10 smaller fragments. Weight and width were the only parameters that needed to be divided by 10. The code then iterated through each the penetration equations for each of the smaller fragments.

The entire code was nested in a loop structure that iterated through thickness multipliers (coefficients) until the value for the residual velocity was within 2% of the experimental value. The initial value for the thickness coefficient was unity, increasing in value each iteration by increments of 0.05. A temporary modification of this program redefined the stopping criteria in residual kinetic energy instead of residual velocity in an attempt to improve the code's effectiveness in providing a solution.

The residual velocities and kinetic energy for each fragment are output to the spreadsheet. In addition, data for the whole fragment is output to the spreadsheet. Residual velocity for the whole fragment was calculated from the mean of the smaller fragments. Residual kinetic energy was then calculated using the residual velocity value.

Testing

The Thickness Coefficient Solver program was tested against the UDM to determine if the new code was providing comparable results. This test was done before the addition of the solver loop (when the program was essentially the similar to the UDM) but calculating 10 small fragments instead of one large one. Input data from five shots was tested in both codes, and the resulting residual velocities are shown in Table 4.

TABLE 4. Comparison of Residual Velocities for the UDM and Thickness Coefficient Solver.

Shot	Residual velocity		Difference, %
	UDM	Thickness coefficient solver	
16	330	325	1.53
17	479	476	0.63
17B	534	530	0.75
19	519	518	0.19
20	817	816	0.12

The percentage difference between output values are very small (less than 2%) and was determined to be caused by rounding-error from dividing both the weight and width by 10 to solve for the smaller fragments. This was later verified by dividing both the width and weight of the input data in the UDM, which yielded the exact same results as the modified program.

THICKNESS COEFFICIENT SOLVER WITH LINEAR WEIGHT DISTRIBUTION

This program was a further modification of the UDM and is identical to the Thickness Coefficient Solver with the exception of not having an equal weight distribution for the smaller fragments. Linear Weight Distribution refers to the linear equation used to calculate the weight of each fragment. The weight increases linearly from the outer fragments (numbers 1 and 10) to the inner fragments (numbers 5 and 6), from values of 3.33% to 16.67% of the total weight, respectively. Figure 4 shows a comparison between equally weighted fragments and fragments with linearly distributed weight. The slope (m) and intercept (b) values used in this study were

Fragments 1-5: m=1/30 and c=0
Fragments 6-10: m=-1/30 and c=110/300

The additional lines of code in the Thickness Coefficient Solver are listed in Appendix C.

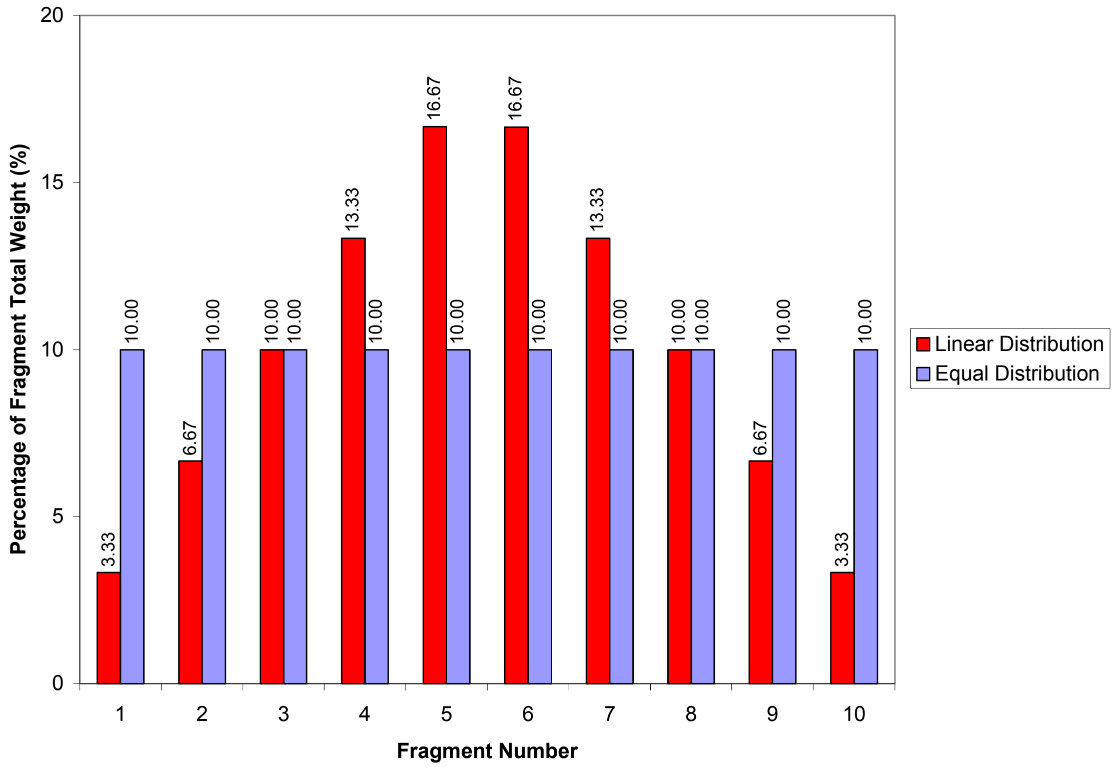

FIGURE 4. Comparison of Small Fragment Weight Distribution.

RESULTS

The results are presented in two categories: solving for the impactor as several smaller fragments, and solving for the impactor as one large fragment.

SOLVING THE IMPACTOR AS SEVERAL SMALLER FRAGMENTS

This first phase of the study attempted to find a method of solving for the impactor as several smaller fragments. Several methods were attempted, but no clear solution was found mostly because of the shortage of data points.

Thickness Coefficient for Entire Width of Structural Element

The Thickness Coefficient Solver code was run using data from the 11 good test shots and structural impact locations shown in Table 2. This code had been designed to vary the thickness coefficient to produce a residual velocity identical to the one achieved experimentally. Figure 5 shows a plot of the calculated thickness coefficient as a function of the percentage of large fragment surface that contacted a structural element. A linear curve fit has been applied to each structural type. The three structural types encountered in this test have formed three distinct regions. However, attempting to curve fit too small a number of data points does not account for the possibility of wild data points.

The code did not arrive at a solution for shots 4, 21, and 32. With shots 4 and 21, only 10% of the large fragment contacted the structural element. For these shots, the thickness of the structural component was increased until the code reached a *no penetration* condition for the one smaller fragment that managed to impact. With the residual velocity of this fragment at 0 ft/s, the mean residual velocity of the other nine fragments was sufficiently high enough not to meet the stopping criteria. With the residual velocity of the one fragment already at 0 ft/s and unable to go any lower, the thickness coefficient increases with each iteration and the program never arrives at a solution. This was a continual shortcoming of this code because of the method used to determine residual velocity for the entire fragment. In a similar manner, shot 32 had 50% of the fragment contact the rib, but the code was unable to achieve the experimental residual velocity of 1 ft/s.

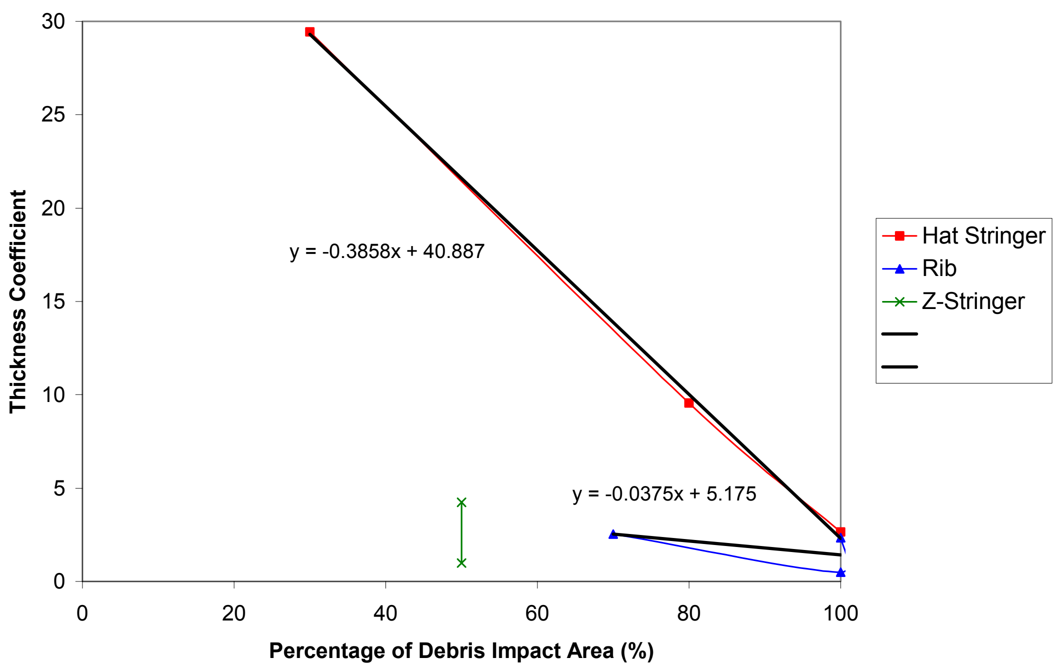

FIGURE 5. Thickness Coefficients for Entire Width of Structural Element of All Structural Elements.

Thickness Coefficient for Base Width of Structural Element

This study was similar to the previous, but used the structural impact locations in Table 3. Only 10 shots with good data could be used; shot 4 could not be included because the large fragment did not impact the base of the z-stringer. The code was unable to determine a solution for shots 4, 11, 21, and 32. The causes of this failure are described in the previous section.

The base-width criteria yielded considerably different results from the entire-width. Figure 6 compares the results between the two structural element width criteria for the hat stringer. The lack of a sufficient number of data points is evident from this plot. However, the direction of the slope for the base-width criteria curve makes more intuitive sense. As the percentage of structural element in contact with the impactor is decreased, the effect on the residual velocity should be less.

Figure 7 plots the results for the rib. This plot shows that both curves are in the same location, due to the width criteria for rib (Figure 2) where the base width for this structural type is the same as the entire width. The results for the z-stringer are presented in Figure 8. The results for z-stringer appear in a similar region of the plot. Again, there are too few data points to draw any conclusions. All three structural types are plotted in Figure 9 for both width criteria.

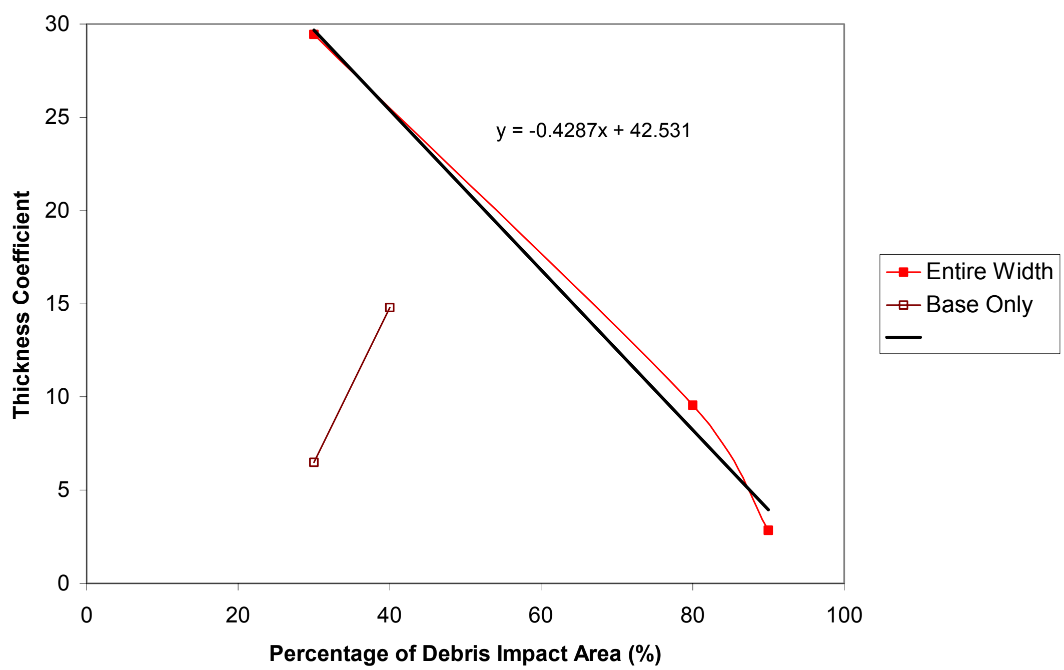

FIGURE 6. Comparison of Thickness Coefficient for Base Width and Entire Width of Hat Stringer.

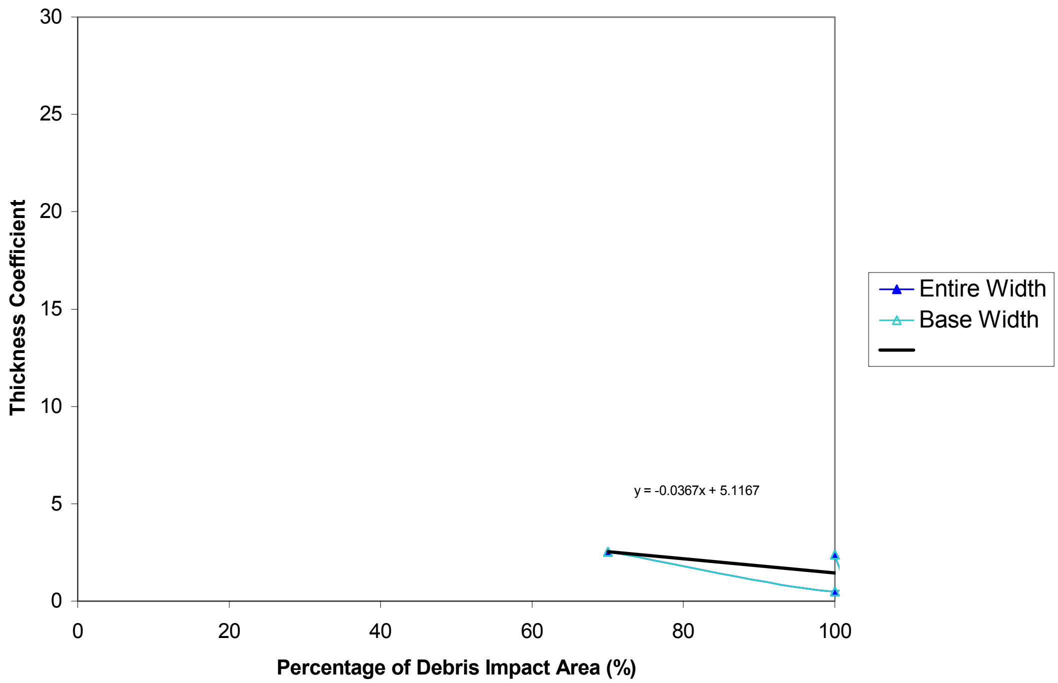

FIGURE 7. Comparison of Thickness Coefficients for Base Width and Entire Width of Rib.

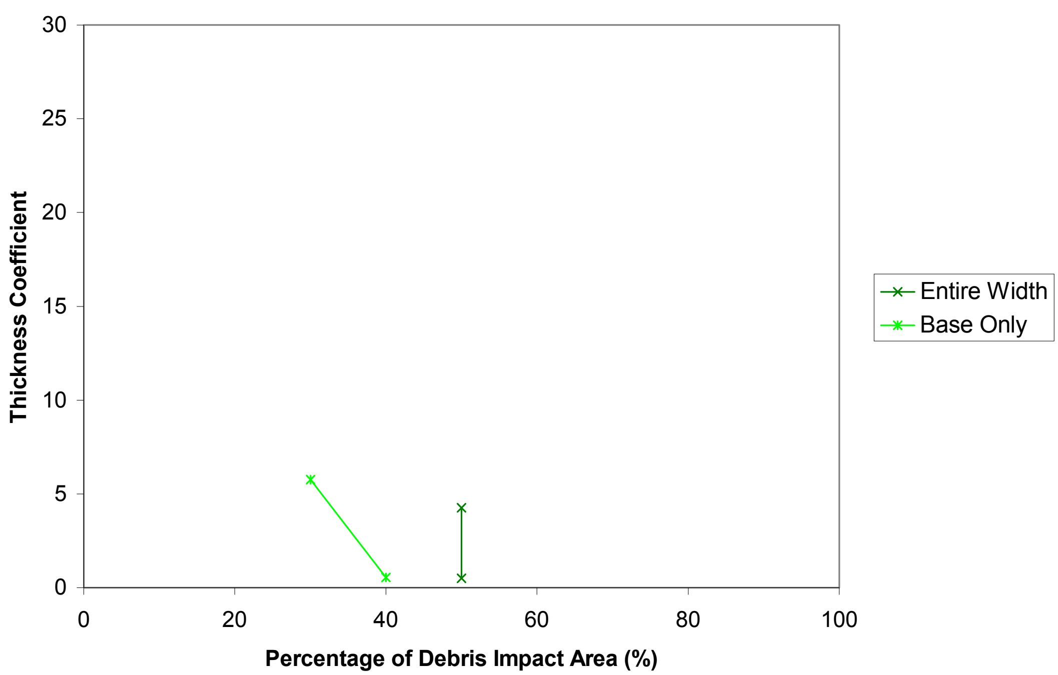

FIGURE 8. Comparison of Thickness Coefficient for Base Width and Entire Width of Z-Stringer.

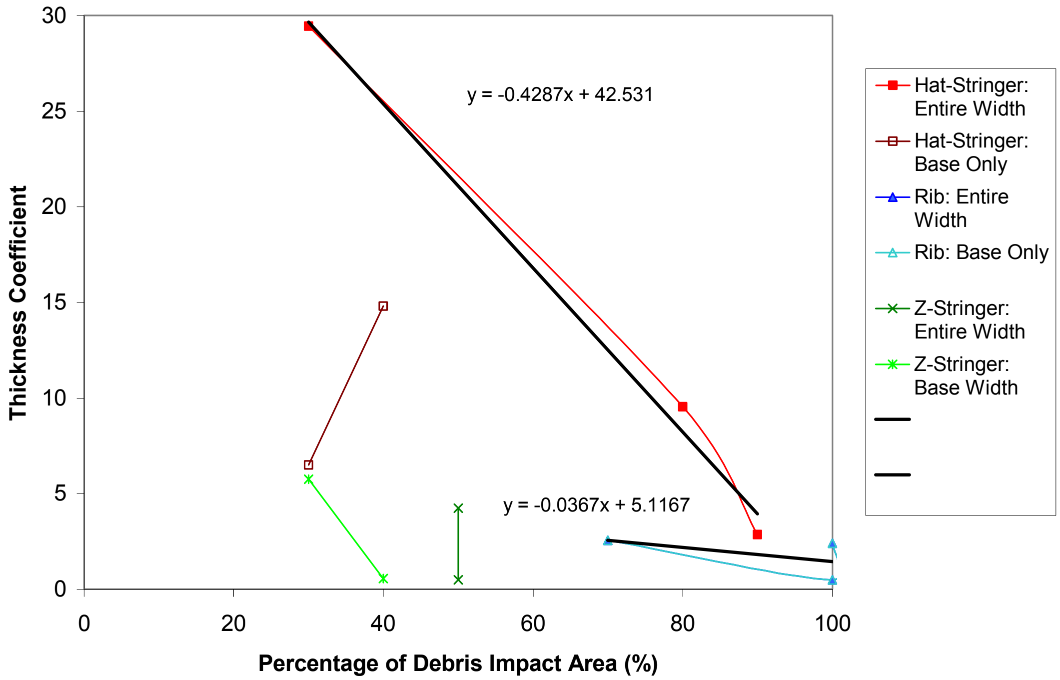

FIGURE 9. Comparison of Thickness Coefficients for Base and Entire Width of All Structural Elements.

Thickness Coefficient for Base Width of Structural Element with New Stopping Conditions

The temporary modification of the Thickness Coefficient Solver to use residual kinetic energy as the stopping condition was done in an attempt to reduce the number of data points that do not reach a solution. All three structural types were run with the code using both width criteria. A comparison of the results between the V_{res} and KE_{res} stopping conditions is shown in Tables 5 and 6, for the entire width and base width criteria. The tables show that the solutions are very similar. Any disparity in the results is due to the iteration step size and the improved accuracy of the KE_{res} stopping condition because of the V_{res}^2 term. This modification did not improve on the code's inability to obtain a solution for some shots.

Thickness Coefficient for Base Width of Structural Element with a Linear Weight Distribution

This analysis was a further attempt to find a consistent relationship between the amount of the impactor making contact with a structural member and a multiple of its thickness. All three structural types were run with the code using both width criteria. The code diverged on almost twice as many solutions as the version with an equal weight distribution but yielded very different results. Table 7 lists the thickness coefficients solved for using the entire width criterion. The percent difference column is shown for comparison. The results of the code using the base width criterion are shown in Table 8.

TABLE 5. Comparison of Results Between V_{res} and KE_{res} Stopping Conditions for Entire Width.

Shot	Structural component	Thickness coefficient		Difference, %
		V_{res} stopping conditions	KE_{res} stopping conditions	
4	Z-Stringer	No Solution	No Solution	N/A
8	Z-Stringer	4.25	4.40	3.47
9	Z-Stringer	0.50	0.65	26.09
11	Hat Stringer	29.45	29.80	1.18
13	Rib	2.55	2.65	3.85
14	Rib	0.50	0.55	9.52
15	Rib	2.40	2.40	0.00
21	Rib	No solution	No solution	N/A
22	Hat Stringer	2.85	3.30	14.63
26B	Hat Stringer	9.55	10.05	5.10
32	Rib	No solution	No solution	N/A

TABLE 6. Comparison of Results Between V_{res} and KE_{res} Stopping Conditions for Base Width.

Shot	Structural component	Thickness coefficient		Difference, %
		V_{res} stopping conditions	KE_{res} stopping conditions	
4	Z-Stringer	No solution	No solution	N/A
8	Z-Stringer	5.75	5.90	2.58
9	Z-Stringer	0.55	0.75	30.77
11	Hat Stringer	No solution	No solution	N/A
13	Rib	2.55	2.65	3.85
14	Rib	0.50	0.55	9.52
15	Rib	2.40	2.40	0.00
21	Rib	No solution	No solution	N/A
22	Hat Stringer	6.50	7.35	12.27
26B	Hat Stringer	14.80	15.50	4.62
32	Rib	No solution	No solution	N/A

TABLE 7. Comparison of Results Between Equal and Linear Weight Distribution for Entire Width.

Shot	Structural component	Thickness coefficient		Difference, %
		Equal weight distribution	Linear weight distribution	
4	Z-Stringer	No solution	No solution	N/A
8	Z-Stringer	4.25	1.70	85.71
9	Z-Stringer	0.50	No solution	N/A
11	Hat Stringer	29.45	No solution	N/A
13	Rib	2.55	1.10	79.45
14	Rib	0.50	No solution	N/A
15	Rib	2.40	0.90	90.91
21	Rib	No solution	No solution	N/A
22	Hat Stringer	2.85	1.70	50.55
26B	Hat Stringer	9.55	6.55	37.27
32	Rib	No solution	No solution	N/A

TABLE 8. Comparison of Results Between Equal and Linear Weight Distribution for Base Width.

Shot	Structural component	Thickness coefficient		Difference, %
		Equal weight distribution	Linear weight distribution	
4	Z-Stringer	No solution	No solution	N/A
8	Z-Stringer	5.75	5.65	1.75
9	Z-Stringer	0.55	No Solution	N/A
11	Hat Stringer	No solution	No solution	N/A
13	Rib	2.55	1.10	79.45
14	Rib	0.50	No Solution	N/A
15	Rib	2.40	0.90	85.71
21	Rib	No solution	No solution	N/A
22	Hat Stringer	6.50	5.45	17.57
26B	Hat Stringer	14.80	18.85	24.07
32	Rib	No solution	No solution	N/A

SOLVING THE IMPACTOR AS ONE LARGE FRAGMENT

The second phase of the study attempted to find a relationship from the test data. As with the smaller fragments, the large fragment study failed to provide successful results.

Percentage of Impactor Contacting the Structural Element and the Change in Kinetic Energy

This study plotted the change in the impactor's kinetic energy (KE) with respect to the percentage of the impactor that contacted a structural element. Both the entire- and base-width criteria (from Tables 2 and 3, respectively), were used. Figure 10 shows the change in KE for an impact involving a hat stringer. The three data points for the hat stringer typically provide consistent data. The change in KE for the rib is shown in Figure 11. The scale on this plot has been increased due to the dispersion of the data points. This data does not show any consistent relationship for the rib. The z-stringer is shown in Figure 12. The three data points for the entire width curve are the result of the inclusion of shot 4, which barely touched the z-stringer but not enough to meet the base width criterion. All structural elements are plotted in Figure 13. This plot shows some consistency in the z-stringer and hat stringer data; however, the rib data is very erratic and widely dispersed.

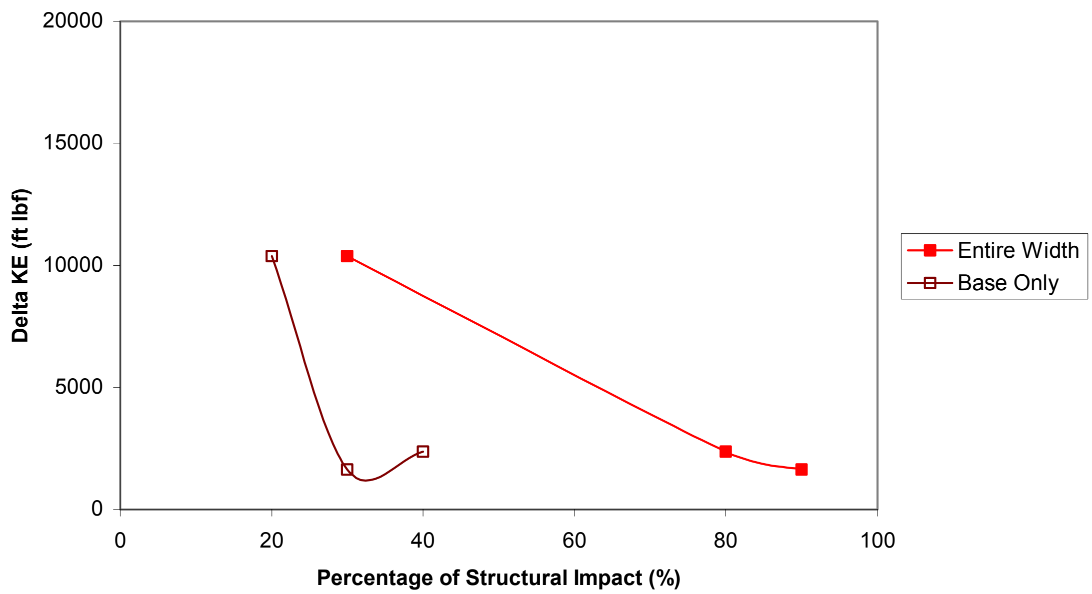

FIGURE 10. Change in Kinetic Energy for Base Width and Entire Width of Hat Stringer.

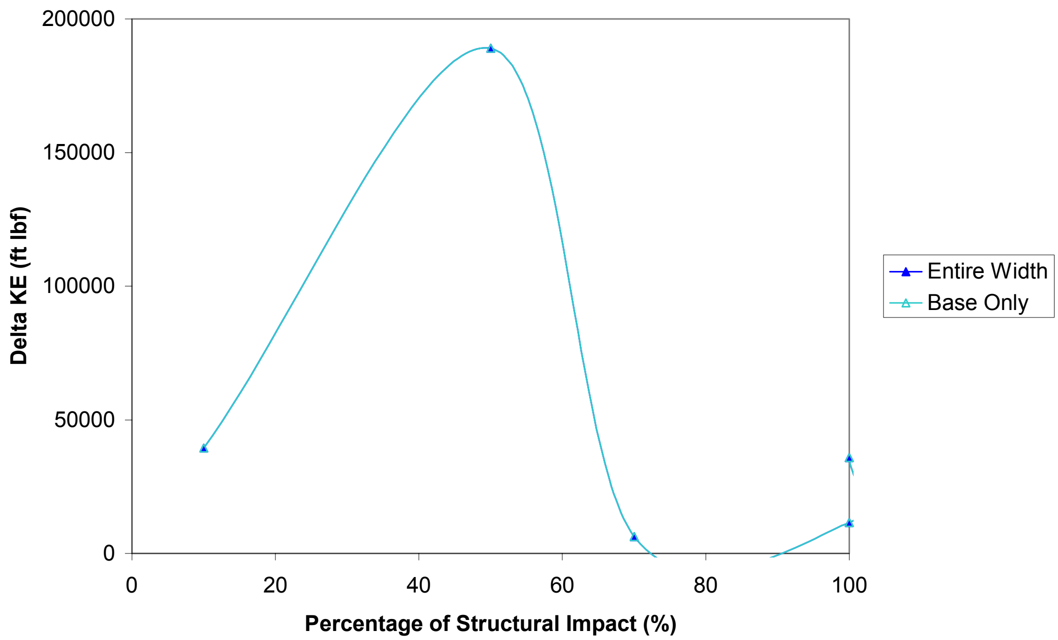

FIGURE 11. Change in Kinetic Energy for Base Width and Entire Width of Rib.

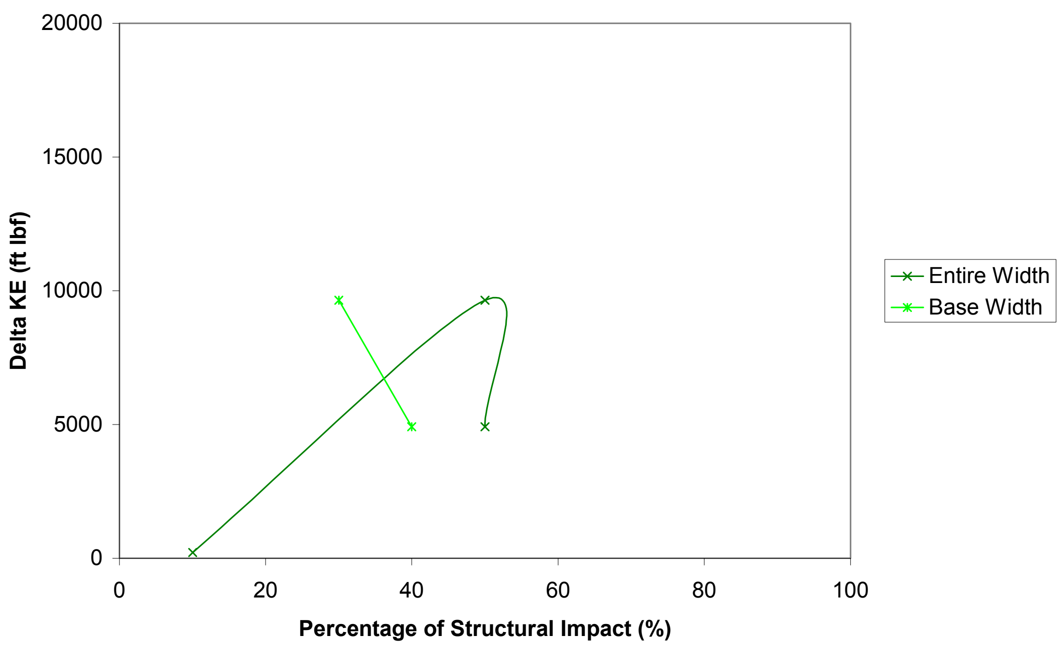

FIGURE 12. Change in Kinetic Energy for Base Width and Entire Width of Z-Stringer.

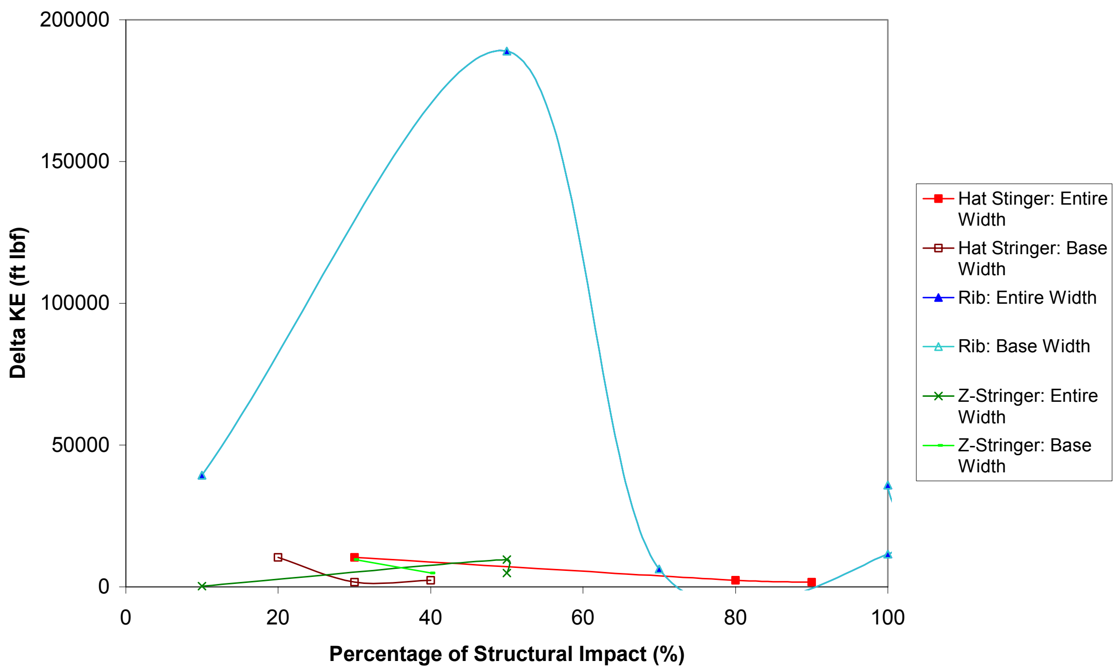

FIGURE 13. Change in Kinetic Energy for Base Width and Entire Width of All Structural Elements.

Initial Velocity with Respect to the Change in Kinetic Energy

The initial velocity of the fragment was plotted with respect to the change in KE (Figure 14). This analysis yielded similar trends as the preceding. The rib structure showed no consistency and the plot provided no noticeable trends.

Presented Area Ratio with Respect to the Prediction Accuracy

The effectiveness of the UDM program was studied by plotting the area ratio with respect to the prediction accuracy. Figure 15 shows how the UDM program predicts the residual velocity with considerable accuracy for skin-only shots. However, there were some skin-only shots that were not correctly predicted. The introduction of fuel tubing had only a slight effect on the residual velocity, thereby implying that correction factors need not be applied. Solutions for impacts involving structural members appeared reasonable until the area ratio exceeded 0.15. This result implies that the closer the impactor is to being perpendicular to the impacting surface, the more accurately the UDM can predict a solution.

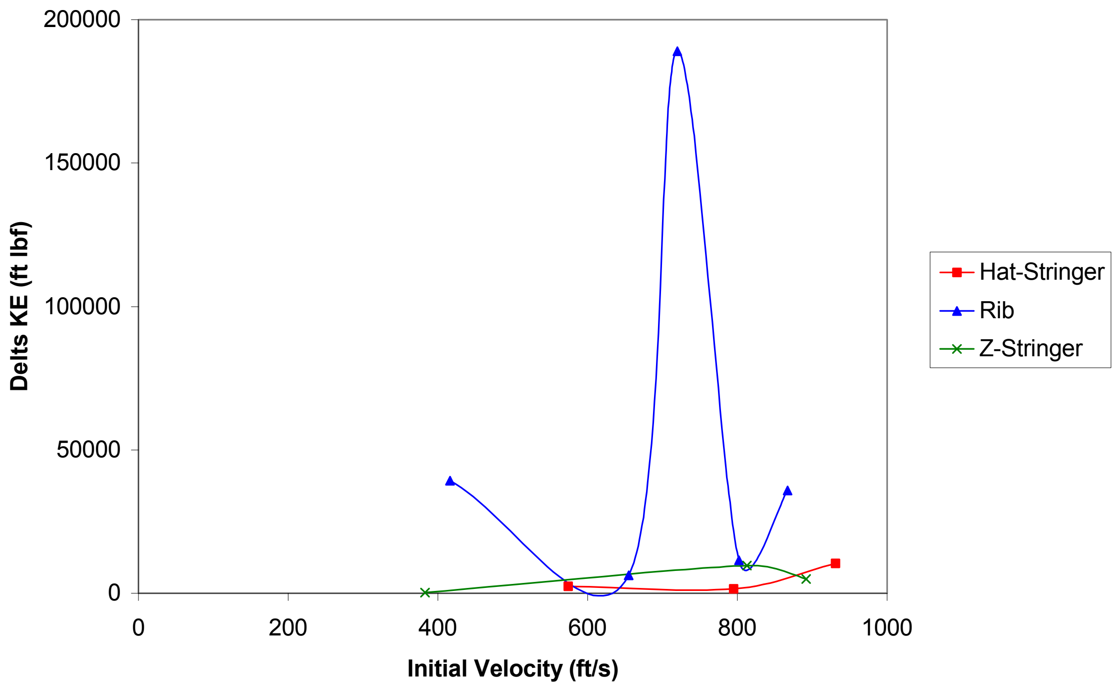

FIGURE 14. Comparison of Initial Velocity to the Change in Kinetic Energy for All Structures.

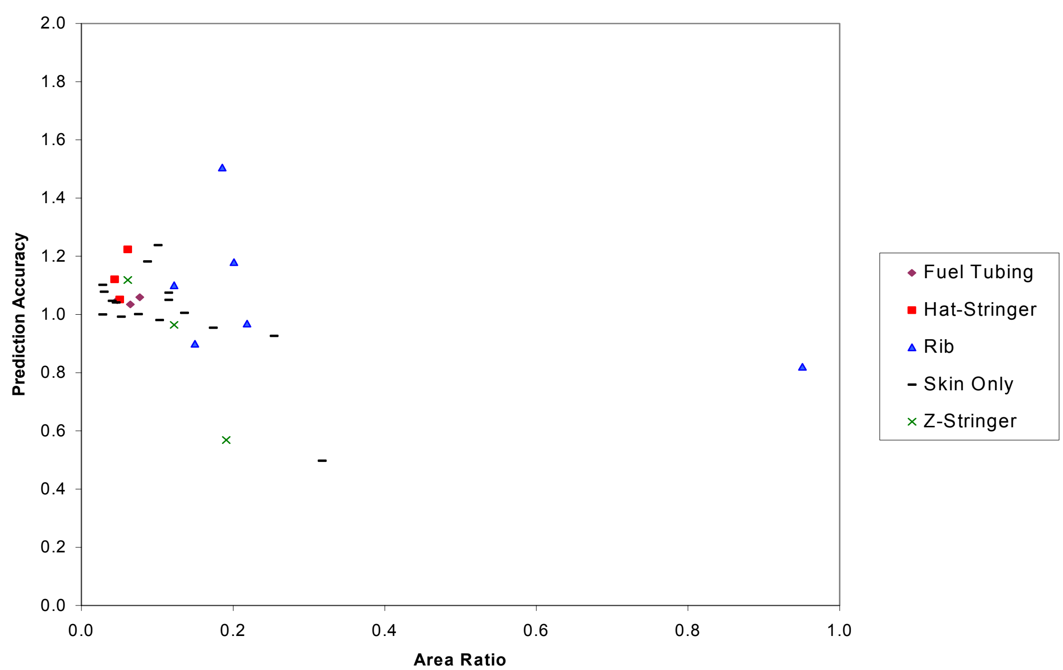

FIGURE 15. Comparison of Prediction Accuracy with Respect to Area Ratio.

Five shots had prediction accuracies either lower than 0.8 or higher than 1.2. A prediction accuracy lower than 1 is the result of the UDM predicting a residual velocity lower than what actually occurred during the experiment. Shots 4 (skin and z-stringer) and 24 (skin only) had prediction accuracies lower than 0.8. Neither shot appears to have obscure input parameters. Shots 11, 32, and 35 had prediction accuracies higher than 1.2, which defines them as having lower residual velocities than the UDM predicted. Shot 11 impacted a hat-stringer and shot 32 a rib, while shot 35 was skin only. For shot 32, the experimental residual velocity was 1 ft/s, which is extremely low in comparison to all other shots.

CONCLUSIONS

This analysis was unable to provide any firm improvements to the existing UDM program because of the insufficient number of data points. Intuitively, the most effective method of modeling fragment impacts with structural elements is to break the fragment into smaller pieces. Only those fragments that impact the structural element should consider the component's effects.

When sufficient data exists on structural impacts, the Thickness Coefficient Solver code can be run. This data can then be plotted and a curve-fit applied. Any linear or polynomial relationship can then be added to the existing UDM code.

REFERENCES

1. J. Manchor and C. Frankenburger. *Engine Debris Penetration Testing*. DOT/FAA/AR-99/19, June 1998.

Appendix A

UNCONTROLLED DEBRIS MODEL (UDM)

Excel Spreadsheet and Code

This page intentionally left blank.

INPUTS

Fragment Simulator
Turbine Blade Fragment

1gm= 2.21E-03 lbm

			No. of Plates	1				Material
Width	2.75	in	plate thickness 1	0.085	in	Frag. Ang. 1	87.7	1
Height	4.75	in	plate thickness 2	0	in	Frag. Ang. 2	89	1
Weight Frag	2.80E-01	lbf	plate thickness 3	0	in	Frag. Ang. 3	0	1
Release Vel.	658	ft/s	plate thickness 4	0	in	Frag. Ang. 4	0	1
Obliquity	8	deg	plate thickness 5	0	in	Frag. Ang. 5	0	1
			plate thickness 6	0	in	Frag. Ang. 6	0	1
			plate thickness 7	0	in	Frag. Ang. 7	0	1
			plate thickness 8	0	in	Frag. Ang. 8	0	1
			plate thickness 9	0	in	Frag. Ang. 9	0	1
			plate thickness 10	0	in	Frag. Ang. 10	0	1

Plate	***V50*** (ft/s)	***Vr*** (ft/s)	***Residual Energy*** (ft lbf)	***tr*** (in)	***KE ratio***	***Delta Velocity*** (ft/s)	***Presented Area*** (sq. in.)
1	73.9	644	1805.3	0.93	0.96	14.4	0.52

Vr Req'd (ft/s)	thickness (in)	Vr Calc (ft/s)	Goal Delta Vr
75	0.085	380	305

Material	Al 2024 T3	Hard Steel	Ti
density (grains / in^3)	701	1950	1134
Cbf (m/s)	413	964	491
bf	0.941	0.963	1.314
h	1.098	1.286	1.643
f	-0.038	-0.057	0.011

```
'Top of Module
' Modified by Chuck Frankenberger 5/23/97
Sub ResVel()
   'Activate UI sheet
   ThisWorkbook.Sheets("Interface").Activate
   Set transrng = Worksheets("Interface").Cells(1, 1).CurrentRegion
   Set MatRng = Worksheets("Materials").Cells(1, 1).CurrentRegion
   Dim thick(10), angle(10)
   Dim material(10) As Integer
   'Delete previous run
   Range("a17:h26").Select
   Selection.ClearContents
   Range("B8").Select

   w = transrng.Cells(4, 2).Value          'debris width
   d = transrng.Cells(5, 2).Value          'debris height
   mass = transrng.Cells(6, 2).Value       'debris mass
   Velo = transrng.Cells(7, 2).Value       'debris initial velocity
   theta = transrng.Cells(8, 2).Value     'maximum trajectory angle
   noofplt = transrng.Cells(3, 6).Value   'number of plates

   For i = 1 To noofplt

   thick(i) = transrng.Cells(3 + i, 6).Value   'plate i thickness
   angle(i) = transrng.Cells(3 + i, 9).Value   'Frag i orientation
   material(i) = transrng.Cells(3 + i, 10).Value 'material for plate i
   g = 32.174

   Next
   'Preliminary Calculations
   mass = mass * 7000             'convert from lbm to grains
   KEo = 0.5 * (mass / (7000 * g)) * Velo ^ 2
   Pi = 3.1415927

   j = 1
   Vdeb = Velo
   Do Until j > noofplt

     rho = MatRng.Cells(2, material(j) + 1).Value  'plate density
     Cbf = MatRng.Cells(3, material(j) + 1).Value
     bf = MatRng.Cells(4, material(j) + 1).Value
     h = MatRng.Cells(5, material(j) + 1).Value
     f = MatRng.Cells(6, material(j) + 1).Value

       Ap = Cos(angle(j) * Pi / 180) * w * d
```

```
        K = 3.2808399 * Cbf * (1 / Cos(theta * Pi / 180)) ^ h * (1980 * Ap / mass) ^ bf *
(1980 * Ap / 100) ^ f
        Q8 = 1980 * thick(j) * Ap / mass
        Q11 = Q8 * mass / 100
        V50 = 3.2808399 * Cbf * Q8 ^ bf * (1 / Cos(theta * Pi / 180)) ^ h * Q11 ^ f
        Q4 = rho * Ap * thick(j) / (mass * Cos(theta * Pi / 180))

    'estimate plate thicknesses for V50

      If Vdeb > V50 Then
         Vr = (Vdeb ^ 2 - V50 ^ 2) ^ 0.5 / (1 + Q4)
         tr = (Vr / K) ^ (1 / (bf + f))
      Else
         Vr = 0
         tr = 0                    'no penetration
      End If
      KE = 0.5 * (mass / (7000 * g)) * Vr ^ 2
      KEratio = KE / KEo

    'Print Results
      transrng.Cells(16 + j, 1).Value = j
      transrng.Cells(16 + j, 2).Value = V50
      transrng.Cells(16 + j, 3).Value = Vr
      transrng.Cells(16 + j, 4).Value = KE
      transrng.Cells(16 + j, 5).Value = tr
      transrng.Cells(16 + j, 6).Value = KEratio
      transrng.Cells(16 + j, 7).Value = Vdeb - Vr
      transrng.Cells(16 + j, 8).Value = Ap
      Vdeb = Vr
      j = j + 1
    Loop


End Sub
'
'
'
```

Appendix B

THICKNESS COEFFICIENT SOLVER

Excel Spreadsheet and Code

This page intentionally left blank.

Impactor Global Specifications		
Shot No.	22	-
Width	2.875	in
Height	7.875	in
Weight	302.5	g
Velocity	795	ft/s
Obliquity	14	deg
Frag Angle	87.1	deg

Color Key	
(grey)	Input Field
(cyan)	Output Field

Impacted Surface Data	Thickness in	Material Code*
Plate	0.1000	1
Rib/Stringer	0.0680	1

*See Materials worksheet

Experimental Results		
Res. Velocity	725.00	ft/s

Real-Time Iteration Monitor		
Counter	Coefficient	%Difference
121	6.50	1.95

Impactor Local Specifications		
Location Number	Location Percentage	Number of Surfaces
1	0-10%	1
2	11-20%	1
3	21-30%	2
4	31-40%	2
5	41-50%	2
6	51-60%	1
7	61-70%	1
8	71-80%	1
9	81-90%	1
10	91-100%	1

Local Output Data

Location Number	Surface Number	V50 ft/s	Residual Velocity ft/s	Residual KE ft lbf	tr in	KE Ratio	Delta Velocity ft/s	Presented Area sq. in
1	1	86.04	776.57	625.11	1.1431	0.9542	18.43	0.11
2	1	86.04	776.57	625.11	1.1431	0.9542	18.43	0.11
	1	86.04	776.57	625.11	1.1431	0.9542	18.43	0.11
	2	329.25	652.22	440.94	0.9423	0.6731	142.78	0.11
4	1	86.04	776.57	625.11	1.1431	0.9542	18.43	0.11
	2	329.25	652.22	440.94	0.9423	0.6731	142.78	0.11
	1	86.04	776.57	625.11	1.1431	0.9542	18.43	0.11
	2	329.25	652.22	440.94	0.9423	0.6731	142.78	0.11
	1	86.04	776.57	625.11	1.1431	0.9542	18.43	0.11
	1	86.04	776.57	625.11	1.1431	0.9542	18.43	0.11
	1	86.04	776.57	625.11	1.1431	0.9542	18.43	0.11
	1	86.04	776.57	625.11	1.1431	0.9542	18.43	0.11
	1	86.04	776.57	625.11	1.1431	0.9542	18.43	0.11
Totals		159.01	739.26	5664.94		0.8647	55.74	1.15

Material	Al 2024 T3	Hard Steel	Ti
density (grains / in^3)	701	1950	1134
Cbf (m/s)	413	964	491
bf	0.941	0.963	1.314
h	1.098	1.286	1.643
f	-0.038	-0.057	0.011

```
' THICKNESS COEFFICIENT SOLVER
'
' Modified by Chuck Frankenberger 5/23/97
' Modified by Richard Mueller 1/13/00
'
' This program is a modification of the fragment penetration
' equations program, written by Chuck Frankenberger. This
' program iterates to detemine a thickness coefficient that
' will produce a residual velocity within 2% of the actual
' residual velocity from a test.
'
' Definition of Program Variables
'
'     Variable    Description (units)
'
'     angle       Fragmentation Angle (degrees)
'     Ap          Impactor Presented Area (in^2)
'     AreaP(10)   Impactor Local Presented Area (in^2)
'     bf          Material Properties Variable
'     Cbf         Material Properties Variable
'     d           Impactor Length (in)
'     dV          Change in Impactor Velocity (ft/s)
'     deltaV(10)  Local Change in Impactor Velocity (ft/s)
'     f           Material Properties Variable
'     g           Acceleration Due to Gravity (ft/s^2)
'     h           Material Properties Variable
'     i           Cell Location Pointer (integer)
'     j           Plate Number (integer)
'     k           Counter (integer)
'     K           Penetration Equation Variable
'     KE          Impactor Kinetic Energy (ft lbf)
'     KE0         Impactor Initial Kinetic Energy (ft lbf)
'     KEratio     Ratio of Impactor Initial and Residual KE (unitless)
'     kntr        Fragment Number (integer)
'     m           Thickness coefficient (unitless)
'     material(2) Surface Material Code (integer)
'     n           Iteration Counter (integer)
'     noofplt     Number of Plates (integer)
'     PercentDiff Percent Difference (%)
'     Q4          Penetration Equation Variable
'     Q8          Penetration Equation Variable
'     Q11         Penetration Equation Variable
'     rho         Density (grains/in^3)
'     setbit      Structural Impact Identifier (integer)
'     theta       Obliquity Angle (degrees)
'     thick(10)   Local Surface Thickness (in)
```

```
'       thickness   Surface thickness (in)
'       V50         Impactor 50% Velocity (ft/s)
'       Vdeb        Impactor Residual Velocity (ft/s)
'       Vel0        Impactor Initial Velocity (ft/s)
'       Vel50(10)   Impactor Local 50% Velocity (ft/s)
'       Vr          Impactor Residual Velocity (ft/s)
'       Vres(10)    Impactor Local Residual Velocity (ft/s)
'       Vresexp     Experimental Impactor Residual Velocity (ft/s)
'       w           Impactor Width (in)
'       weight      Impactor Weight (lbf)
'       weight_g    Impactor Weight (grams)
'       weight_gr   Impactor Weight (grains)
'
Sub ResVel()
    'Activate UI sheet
    ThisWorkbook.Sheets("Interface").Activate
    'Declare worksheets
    Set transrng = Worksheets("Interface").Cells(1, 1).CurrentRegion
    Set MatRng = Worksheets("Materials").Cells(1, 1).CurrentRegion
    'Declare arrays
    Dim thick(2), Vres(10), deltaV(10), AreaP(10), Vel50(10)
    Dim material(2) As Integer
    'Initialize variables
    n = 1
    m = 1
    setbit = 0
    PercentDiff = 10
    'Solver loop
    Do Until PercentDiff < 2
        'Delete previous run
        Range("a20:i40").Select
        Selection.ClearContents
        Range("B8").Select
        'Input impactor global specifications
        w = transrng.Cells(4, 2).Value
        d = transrng.Cells(5, 2).Value
        weight_g = transrng.Cells(6, 2).Value
        Vel0 = transrng.Cells(7, 2).Value
        theta = transrng.Cells(8, 2).Value
        angle = transrng.Cells(9, 2).Value
        'Input impacted surface specifications
        For i = 1 To 2
            thick(i) = transrng.Cells(3 + i, 6).Value
            material(i) = transrng.Cells(3 + i, 7).Value
        Next
        'Convert grams to lbf
```

```
Weight = weight_g * 0.002205
'Convert lbf to grains
Weight_gr = Weight * 7000
'Define impactor local conditions
w = w / 10
Weight = Weight / 10
Weight_gr = Weight_gr / 10
'Calculation of initial kinetic energy
g = 32.174
KE0 = 0.5 * (Weight / g) * Vel0 ^ 2
'Iterate through each impactor location
For kntr = 1 To 10
   'Determine the number of surfaces at impactor location
   noofplt = transrng.Cells(3 + kntr, 11).Value
   j = 1
   Vdeb = Vel0
   'Iterate through each impact surface
   Do Until j > noofplt
      'Read material properties
      rho = MatRng.Cells(2, material(j) + 1).Value
      Cbf = MatRng.Cells(3, material(j) + 1).Value
      bf = MatRng.Cells(4, material(j) + 1).Value
      h = MatRng.Cells(5, material(j) + 1).Value
      f = MatRng.Cells(6, material(j) + 1).Value
      'Set surface thickness
      If j = 1 Then
         thickness = thick(1)
      ElseIf j = 2 Then
         thickness = m * thick(2)
         setbit = 1
      End If
      'Penetration Equations
      Pi = 3.1415927
      Ap = Cos(angle * Pi / 180) * w * d
      K = 3.2808399 * Cbf * (1 / Cos(theta * Pi / 180)) ^ h * (1980 * Ap /
         Weight_gr) ^ bf * (1980 * Ap / 100) ^ f
      Q8 = 1980 * thickness * Ap / Weight_gr
      Q11 = Q8 * Weight_gr / 100
      V50 = 3.2808399 * Cbf * Q8 ^ bf * (1 / Cos(theta * Pi / 180)) ^ h * Q11 ^ f
      Q4 = rho * Ap * thickness / (Weight_gr * Cos(theta * Pi / 180))
      'Estimate plate thicknesses for V50 and determine whether penetration occurs
      If Vdeb > V50 Then
         Vr = (Vdeb ^ 2 - V50 ^ 2) ^ 0.5 / (1 + Q4)
         tr = (Vr / K) ^ (1 / (bf + f))
      Else
         Vr = 0
```

```
            tr = 0
        End If
        'Calculate residual kinectic energy and kinetic energy ratio
        KE = 0.5 * (Weight / g) * Vr ^ 2
        KEratio = KE / KE0
        'Output results to spreadsheet
        If kntr = 1 And j = 1 Then
            i = 20
        Else
            i = i + 1
        End If
        transrng.Cells(i, 1).Value = kntr
        transrng.Cells(i, 2).Value = j
        transrng.Cells(i, 3).Value = V50
        transrng.Cells(i, 4).Value = Vr
        transrng.Cells(i, 5).Value = KE
        transrng.Cells(i, 6).Value = tr
        transrng.Cells(i, 7).Value = KEratio
        transrng.Cells(i, 8).Value = Vel0 - Vr
        transrng.Cells(i, 9).Value = Ap
        'Write output to data arrays
        If j = noofplt Then
            Vel50(kntr) = V50
            Vres(kntr) = Vr
            deltaV(kntr) = Vel0 - Vr
            AreaP(kntr) = Ap
        End If
        Vdeb = Vr
        j = j + 1
    Loop
Next
'Calculate mean V50
V50 = 0
For K = 1 To 10
    V50 = V50 + Vel50(K)
Next
V50 = V50 / 10
transrng.Cells(41, 3).Value = V50
'Calculate mean residual velocity
Vr = 0
For K = 1 To 10
    Vr = Vr + Vres(K)
Next
Vr = Vr / 10
transrng.Cells(41, 4).Value = Vr
'Calculate total residual KE
```

```
        weight_g = transrng.Cells(6, 2).Value
        Weight = weight_g * 0.002205
        KE = 0.5 * (Weight / g) * Vr ^ 2
        transrng.Cells(41, 5).Value = KE
        'Calculate total KE ratio
        KE0 = 0.5 * (Weight / g) * Vel0 ^ 2
        KEratio = KE / KE0
        transrng.Cells(41, 7).Value = KEratio
        'Calculate mean delta velocity
        dV = 0
        For K = 1 To 10
            dV = dV + deltaV(K)
        Next
        dV = dV / 10
        transrng.Cells(41, 8).Value = dV
        'Calculate total presented area
        Ap = 0
        For K = 1 To 10
            Ap = Ap + AreaP(10)
        Next
        transrng.Cells(41, 9).Value = Ap
        'Percent Difference
        Vresexp = transrng.Cells(9, 6).Value
        PercentDiff = ((Abs(Vresexp - Vr)) / ((Vresexp + Vr) / 2)) * 100
        'Output real-time data
        transrng.Cells(13, 7).Value = PercentDiff
        transrng.Cells(13, 5).Value = n
        transrng.Cells(13, 6).Value = m
        'Step thickness coefficient
        m = m + 0.05
        'Exit loop if no structural elements are involved
        If n = 2 And setbit = 0 Then
            Exit Do
        End If
        n = n + 1
    Loop
End Sub
```

This page intentionally left blank.

Appendix C

THICKNESS COEFFICIENT SOLVER LINEAR WEIGHT DISTRIBUTION

Additional Code

This page intentionally left blank.

```
'      'Define impactor linear weight distibution
        For kntr = 1 To 5
           Wt(kntr) = (((10/3) * kntr) / 100) * Weight
        Next
        For kntr = 6 To 10
           Wt(kntr) = ((-(10/3) * kntr + (110/3)) / 100) * Weight
        Next
```